

Spring 2018

Foutier Transform Infrared Spectroscopy Instrumentation and Integration with Thermogravimetry

Junjie Xiang

Western Kentucky University, junjiexiangknn@gmail.com

Follow this and additional works at: <https://digitalcommons.wku.edu/theses>



Part of the [Analytical Chemistry Commons](#), and the [Materials Chemistry Commons](#)

Recommended Citation

Xiang, Junjie, "Foutier Transform Infrared Spectroscopy Instrumentation and Integration with Thermogravimetry" (2018). *Masters Theses & Specialist Projects*. Paper 2572.

<https://digitalcommons.wku.edu/theses/2572>

This Thesis is brought to you for free and open access by TopSCHOLAR®. It has been accepted for inclusion in Masters Theses & Specialist Projects by an authorized administrator of TopSCHOLAR®. For more information, please contact topscholar@wku.edu.

FOURIER TRANSFORM INFRARED SPECTROSCOPY INSTRUMENTATION AND
INTEGRATION WITH THERMOGRAVIMETRY

A Thesis
Presented to
The Faculty of the Department of Chemistry
Western Kentucky University
Bowling Green, Kentucky

In Partial Fulfillment
Of the Requirements for the Degree
Master of Science

By
Junjie Xiang

May 2018

FOURIER TRANSFORM INFRARED SPECTROSCOPY INSTRUMENTATION AND
INTEGRATION WITH THERMOGRAVIMETRY

Date Recommended March 28, 2018

Yan Cao

Dr. Yan Cao, Director of Thesis

Bangbo Yan

Dr. Bangbo Yan

D. Dahl

Dr. Darwin Dahl

T. Coffey

Dean, Graduate Studies and Research

4/5/18

Date

I dedicate this thesis to my family and friends.

ACKNOWLEDGEMENTS

I am using this opportunity to express my appreciation and gratitude to those who have helped me during my study and research in the US.

First I want to give my thanks to my research advisor Dr. Cao. His advice, criticisms and corrections provided great guidance and encouragement throughout my research. He has been very successful on delivering concepts of material chemistry. His engineering experience has significant influence on me in designing experiments and solving practical problems. The research work in his lab lifted my implementation capacity and practiced my decision making, which I believe, will be life long benefits for me.

Also I would like to thank Dr. Bangbo Yan and Dr. Darwin Dahl for their willingness to serve as my thesis committee member and their helpful suggestions. I appreciate all their guidance and patience for this thesis and defense. I appreciate Dr. Doug Harper for his patience in LabVIEW classes and his kindly permission and help in the Computational Physics classes and support in my PhD application. I appreciate Dr. Eric Conte for his careful guidance and wonderful lectures in the Advanced Analytical Chemistry classes and his support in my PhD application. Many thanks to Alicia Pesterfield for handling the new orders for lab equipment, to Haley Smith for her countless help and care in school life.

Besides, I want to express my thanks to Gao Hongyan for backing me up when facing the biggest challenges in research and life and providing me with valuable instructions

and advice, to Chen Ying for helping me in applying for WKU, to Li Lin, Cai Chuanchuan, Sui Zifeng, Zhaohai Hong, Zhang Yue, Dong Xinju, Wang Xiaojin who kept me company in the lab, to Wang Yongqing Deng Jiacui and Jiang Fuyin who helped me in capital turnover, to Mark Jessen and his wife Lauren Jessen opened their door to international students and showed us American culture and spiritual truth, to Robin Calamiao, Larry Austin for sharing music and sports, to Craig for teaching me driving, and to all those who have showed kindness and love to me. They have all been very important for my life in Bowling Green in the last two years.

Finally I want to express my gratitude to my family for their endless love and support.

PREFACE

This dissertation is submitted for my Master's degree at Western Kentucky University. The research described in here was instructed by Prof. Yan Cao in the Department of Chemistry, Western Kentucky University, from August 2016 to May 2018 to the best of my knowledge. Except for the acknowledgment and references, this work is original. Neither this, nor any substantially similar dissertation has been or is submitted for any other degree, diploma.

My research of building analytical instrument is an interdisciplinary area of chemistry, electronics, optics and mechanics. The core concept of my research focus is in-situ analysis, instrument integration, spatially resolved and time resolved spectroscopy. The working principles of the analytical instruments interest me a lot. While working in the lab I got familiar with the optics, electronics and also learned how to used the CNC milling machine to make metal parts.

As I see it, in-situ analysis refers to the design of a reactor. Integration of different instrument literally mean how to put them on this reactor. So the key is design a specific reactor and customize the analytical instruments. These ideas turned into two projects: building a FTIR and TG-FTIR. The FTIR project meant to customize the instrument and the thermogravimetry furnace unit was the selected reactor.

I had a little wish that the second project should add an instrument to the WKU list that other students and teacher will able to actually use it. So I made the software very user

friendly. Unfortunately, the control board of the balance broken down for unknown reason beyond repairing after several experiments.

CONTENTS

1 INTRODUCTION.....	1
<i>1.1. Background.....</i>	<i>1</i>
<i>1.2. FTIR Spectroscopy</i>	<i>4</i>
<i>1.3. FTIR instrumentation</i>	<i>6</i>
1.3.1. IR source	6
1.3.2. IR Interferometer	7
1.3.3. IR Detector.....	8
1.3.4. Laser interferometer.....	9
1.3.5. Sample handling.....	10
<i>1.4. Data acquisition and instrument control with LabVIEW.....</i>	<i>11</i>
2 FTIR INSTRUMENTATION PROJECT	14
<i>2.1 Fourier transform and data processing</i>	<i>15</i>
2.1.1 Fourier transform	15
2.1.2 Discrete Fourier transform computation and programming	16
2.1.3 Simulation and FT with LabVIEW.....	19

2.1.4 Simulation with unstable scanning speed	29
2.1.5 Synchronization and test	32
2.2 <i>Hardware setup</i>	36
2.3 <i>Software development</i>	39
3 TG-FTIR PROJECT	47
3.1 <i>Hardware setup</i>	48
3.2 <i>Software Development</i>	50
3.2.1 FTIR Control and Data Transfer	53
3.2.2 TGA Server	57
3.2.3 Main Control	59
3.2.4 Temperature Control	65
3.3 <i>Experimental test</i>	70
3.3.1 Experiment	72
3.3.2 Results and discussion	72
3.3.3 Conclusion	82
4 SUMMARY AND PROSPECT	83

5 LITERATURE CITED85

LIST OF FIGURES

Figure 1. A heated coil IR source with a concave mirror, a micro-machined, electrically modulated thermal infrared emitter	7
Figure 2. Michelson interferometer	8
Figure 3. Synchronization of the IR signal and laser signal(Wikipedia)	9
Figure 4. Sine Wave VI	19
Figure 5. Signal Generation Loop	20
Figure 6. LabVIEW code for Fourier transform	20
Figure 7. FFT Power Spectrum VI	21
Figure 8. Amplitude data for simulation	21
Figure 9. Collection of some of the modulated waves	22
Figure 10. Interferogram simulated.....	22
Figure 11. The FT result of the Python code	11
Figure 12. Fourier transform result of the LabVIEW code	24
Figure 13. Collection of modulated waves(sampling rate 1 kHz).....	25
Figure 14. Interferogram generated (sampling rate at 1 kHz)	25
Figure 15. FT result with a sampling rate of 0.62kHz	27
Figure 16. Main loop for adding stretching and compression points into the IR and laser signal	29

Figure 17. IR and laser data for unsteady scanning. Red line is laser signal and blue line is IR signal	29
Figure 18. FT result with bad interferogram	30
Figure 19. Synchronize loop.....	30
Figure 20. Transition Measurement VI	31
Figure 21. Interferogram before synchronization process	31
Figure 22. Interferogram after synchronization process	32
Figure 23. FT result of the synchronized interferogram	32
Figure 24. The layout of the FTIR optics. The IR source and two detectors are not included in this scope	34
Figure 25. Pyroelectric detector	35
Figure 26. External amplification circuit and diagram.....	36
Figure 27. LabVIEW software project FTIR	36
Figure 28. The Obtain Spectrum state of Main Loop	39
Figure 29. Synchronize VI	40
Figure 30. Motor control action engine block diagram	41
Figure 31. Motor moving status testing code	41
Figure 32. TG-FTIR schematic diagram	44
Figure 33. Hardware setup	45

Figure 34. Inside the DRIFT chamber	45
Figure 35. TG-FTIR project list	46
Figure 36. FTIR Server front panel	49
Figure 37. Detecting New File loop of FTIR Server	50
Figure 38. TCP Server Loop.....	51
Figure 39. Mouse Click Event triggering	51
Figure 40. TGA Server front panel	52
Figure 41. TGA Server block diagram	53
Figure 42. Print Screen VI and Image to Data V I	53
Figure 43. Main Control VI user interface	54
Figure 44. TCP Client Loop for TGA	55
Figure 45. Image to Number VI block diagram.....	56
Figure 46. Number Recognizer front panel. A seven is displayed in a Boolean array indicator	56
Figure 47. Number Recognizer VI block diagram	57
Figure 48. TCP Client Loop for FTIR.....	58
Figure 49. Temperature Control Loop	58
Figure 50. Temperature PID Action Engine VI front panel.....	60

Figure 51. Temperature PID Action Engine VI block diagram	61
Figure 52. Temperature control test, 5 °C/min	62
Figure 53. Temperature control test, 10 °C/min.....	63
Figure 54. Temperature control test, 20 °C/min.....	63
Figure 55. Thermogram of Calcium oxalate decomposition.....	65
Figure 56. Standard Calcium oxalate IR spectrum	67
Figure 57. Correlation of the absorbance and transmittance with the concentration	68
Figure 58. All IR spectra in 3D	69
Figure 59. Comparison plot at wavenumber 3945cm-1	71
Figure 60. Comparison plot at wavenumber 880 cm-1	72
Figure 61. Standard IR spectrum of calcium carbonate	73
Figure 62. Comparison plot at wavenumber 782cm-1	74

FOURIER TRANSFORM INFRARED SPECTROSCOPY INSTRUMENTATION AND INTEGRATION WITH THERMOGRAVIMETRY

Junjie Xiang

May 2018

88 Pages

Directed by: Dr. Yan Cao, Dr. Bangbo Yan, Dr. Darwin Dahl

Department of Chemistry

Western Kentucky University

To discover the potential of IR spectroscopy and explore the details of FTIR instrumentation, a FTIR was built from most basic parts to provide access to every aspect of a IR spectrometer including the hardware and software. The optical system followed the most widely used double-interferometer design. The software control system was developed with LabVIEW to perform data acquisition of the detectors, data processing and controls of the actuators. The FTIR built will be able to provide a full optical IR spectroscopy platform which has a complete control and data acquisition system and can be continuously improved in accuracy and resolution to reach high lab experiment class as the research keep going. The availability of the hardware setup and software source code allows updating of this system for many advanced IR spectroscopy like spatially resolved and time resolved applications.

To achieve in-situ material characterization with multiple measurements, some instruments can be modified and integrated with experiments. This thesis provides a practical and useful example of measuring IR spectra and mass of the sample simultaneously during thermal reactions. This instrument was designed and build with a Fourier transform infrared spectrometer (FTIR) and a thermogravimetric analyzer (TGA). Diffuse reflectance Fourier transform (DRIFT) was equipped to a commercial FTIR to acquire the IR spectra. A micro-balance was taken from a TGA was refitted to this system to measure the sample mass. A series of LabVIEW applications was developed

for the FTIR control and communication, TGA communication and temperature control. The system was successfully built and tested with calcium oxalate decomposition experiments. The data showed that the instrument has good accuracy and repeatability of both the IR and mass measurement. The analysis of the calcium oxalate data demonstrated good correlation between the IR, mass and temperature parameters.

1 INTRODUCTION

1.1. Background

Material chemistry has become one of the most intensively studied fields. The research of material chemistry includes metals and their alloys, semiconductors, insulators, organics (such as polymers to fuels) and etc. There are many exciting developments of new materials cross over the aforementioned categories. For example, the polymer is regularly non-conductive but can be conductive in certain structures which are now widely applied in electronics and renewable energy conversions. There are also many exciting development in the carbon material family, such as two-dimensional graphene and zero-dimensional carbon dot. It is very important to know that many new materials are discovered or created together with the revolution of scientific instruments that enabled scientists to do characterization and other measurements that was not possible before. Generally there are 7 common aspects of the study of a material: structure, crystallography, bonding, properties, synthesis/processing, thermodynamics and kinetics. The process to probe and measure the structure and properties of a material is called characterization. Synthesis, thermodynamics and kinetics study can be sorted as mechanism study. Thus the research work of material chemistry is simplified into two major tasks: material characterization and mechanism study.

There are a lot of tools for material characterization and they mainly includes in two types: microscopy and spectroscopy. These characteristic methods require high precision

instruments. The mechanism study is usually carried out with some macroscopic testings. These tests can usually be done with self built experiment platforms because these data are easier to be measured while the experiment condition varies a lot from one to another making it difficult for a specific instrument to be commercialized.

Most of the time the material characterization is separated from the mechanism study. Almost all microscopy and spectroscopy instruments work only on a static sample in a restricted environment which can not be manipulated to be under a variety of physio-chemistry fields (pressurized, thermal, plasma, radiations and etc.) or special gas environments. Thus many interesting and important information on the change of structures and properties can not be observed and insights on the improvement of material performances are hard to obtain. Those common characterization information only refers to specific situations instead of providing overall view on the life-cycles of a material during its reaction, failure or degradation. It's critical to correlate changes of structure and binding of materials and their spectroscopic responses at some continuous moments of their applications. This requires a combination of the reaction environment and measurement methods, namely, combining mechanism study and material characterization.

There have currently been many good examples on this integration, providing the great insights on properties of materials and their performance in actual applications. For example, Felipe Guzman *et al.* integrated IR and mass spectroscopy on the UV induced ethanol photocatalytic oxidation on TiO₂. Their experiment revealed the many intermediate products produced during the photoreaction on the TiO₂ surface. Mathew Isenberg *et al.* applied both FTIR and UV-Vis in a pulsed adsorption and desorption

experiment system to study the nature of the adsorbed CO₂ on immobilized amine regenerated with utility boiler steam. Results successfully revealed how the metal ions in the steam caused contamination and failure of amine. It is very obvious that UV-Vis and IR spectroscopy are among the most used in-situ characterization methods, because they can work under varied temperatures, pressures and gas environments. Microscopies are generally difficult to be integrated into an actual performance experiment condition, because they require a vacuum environment which left very little option of reaction conditions manipulation. Most recent exciting in-situ techniques addressed applications of SEM/TEM in very specified environment.

A commercial instrument lacks flexibility to adapt to the requirement of in-situ measurement. To achieve in-situ measurement, in most cases an experiment is put into a commercial instrument due to lack of knowledge of how the instrument works, that the instruments can not adapt to the experiment but the experiment has to adapt to the instrument. This is a limitation to the experiment condition. But if one can know the instrument good enough to break it apart and reassemble, it is possible to add the instrument to the experiment platform in one's own fashion. Any instrument involves complicated electronic and software sub-units to achieve automation of instrument control and the data acquisition. In the first chapter the working principle and full set up of hardware and development of software are explained and tested with a project. IR spectroscopy is chosen because it is safe to operate and provides rich structural information of many molecular compounds covering both organics and inorganics. To achieve in-situ measurement a reaction environment is needed. TG (thermogravimetry) is

selected to be integrated with FTIR which not only bring one of the most popular reaction environment but also provides mass information of the sample.

1.2. FTIR Spectroscopy

Spectroscopy is the study of the interaction between matter and electromagnetic radiations. Dependent on electromagnetic wave sources and relative detectors, a series of spectroscopy can be realized for different applications in material research. The region of the electromagnetic wave spectrum usually used are X-ray, UV-Vis, IR (including near IR, mid and far IRs), microwave and T-Hz etc. On the other hand based on the different way the electromagnetic wave interact with the sample different instruments are created. EDX (Energy-dispersive X-ray spectroscopy) examine the X-ray spectrum generated by the sample excited by electron beam or X-ray beam. XRD (X-ray diffraction crystallography) examines the diffraction angle that the sample cause to the incident X-ray. UV-Vis and FTIR studies the absorption of light of the sample.

An UV-Vis spectrometer is very similar with the IR spectrometer in many ways. First they both study the absorbance of the matter. Second they have similar instrumentation. The basic set up includes a light source, a sample chamber and a detector. The key is the wavelength selection part, often called monochromator. Since the detector can only react to the total intensity of the incident light, it is necessary to separate the incident wave according to different wavelengths. In the early times both UV-Vis and IR spectrometer adopted diffraction grating as a monochromator. With a single detector the diffraction grating is accompanied with a motor to move the dispersed spectrum and a slit to select the a wavelength of a certain bandwidth. The width of the slit decides the resolution. The

compact UV-Vis spectrometers adopted diode array or linear CCD (charged coupled device) as the detector, allowing for simultaneous a whole spectrum.

The disadvantages of disperse instrument is that it has relatively low signal noise ratio and it takes long time to finish a scan. The first low-cost dispersive IR spectrometer was commercially available in around 1957 produced by PerkinElmer but FTIR did not become available until 1969 when the computational power of mini-computers became capable of performing the Fourier transform. FTIR was first used in astronomy to observe the weak infrared signal from remote stars. The development of FTIR made a big difference. There are several major advantages of FTIR over a dispersive instrument. A very short movement (eg. 1mm) of the scanning movement in the FTIR is sufficient for the system to recognize the whole spectrum. This means an FTIR can collect a spectrum faster. The FTIR does not have a slit to limit the output wave. Instead all wavelengths are transferred to the detector. It does not improve the resolution by narrower the slit, but achieve high resolution by longer scanning distance. This means the throughput of a FTIR is much higher leading to a good signal noise ratio which can be better than those of a good-quality dispersive instrument usually by more than an order or magnitude. Another advantage of FTIR is its high precision. A laser interferometer is usually adopted in a FTIR system to control the motion of the scanning as well as providing reference for IR sampling. This provides a precision time domain which corresponds to the frequency after Fourier transform. While the dispersive instrument needs external calibration of standards. The spectra of a FTIR are much more comparable than those of a dispersive instrument.

FT instruments also have very good determination of frequency which is very useful when doing subtraction of the background. The optics design of a FT instrument allows a whole wave to pass through to the detector while a dispersive instrument has to use a slit for wave selection that the FT instruments have a much larger energy throughput.

1.3. FTIR instrumentation

The basic components of an FTIR includes the IR source, the Michelson interferometer, the IR detector. It is very common that an FTIR also adopt a laser interferometer for precise signal sampling.

1.3.1. IR source

The IR source is usually inert solid heated to 1200K by current. This covers the mid-IR region(2-25 μm) very well. Silicon carbide is a commonly used material for the inert solid the output of which is similar to a black body. For near-IR (1-2.5 μm) a higher temperature source like a tungsten-halogen lamp is required. For far-IR beyond 50 μm a mercury discharge lamp gives a larger throughput than a thermal source.

In compact IR detection devices some micro IR source are invented. These IR source are inherently a thermal source but the heating part is small enough to fit into a detector size. Due to the small size of the heating element, fast heating and cooling is possible that these IR sources can be modulated electronically instead of using an external wave chopper.

Another relatively new IR source is the quantum cascade laser. A distributed feedback laser is created to generate a single wavelength with a tuning range of less than 0.1% of the central wavelength. Some other types have broader tuning range or are operated as a broad band source. The quantum cascade laser is not a suitable source for FTIR but it is very useful in fast IR spectrum acquisition.



Figure 1. A heated coil IR source with a concave mirror (left), a micro-machined, electrically modulated thermal infrared emitter (right)

1.3.2. IR Interferometer

The interferometer consists of a beamsplitter, a fixed mirror and a moving mirror. Since glass and quartz have strong absorbance in mid-IR, the beamsplitter for FTIR is usually made of potassium bromide or calcium fluoride. Silver, gold, and aluminum mirrors also work for the IR beam.

50% of the beam is designed to be refracted to the fixed mirror and the other 50% transmitted to the moving mirror. The difference of the length of the two arms of the Michelson interferometer is called optical path difference or retardation. By varying the position of the moving mirror, the retardation is changed and the interference pattern of

the IR beam changes accordingly. This IR signal detected in relation to retardation is the interferogram. The signal is at maximum at zero retardation where all wavelengths have constructive interference. The zero retardation is also found with the total constructive feedback.

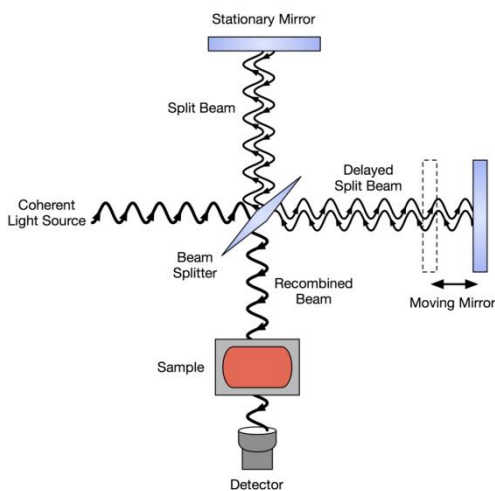


Figure 2. Michelson interferometer(Wikipedia)

1.3.3. IR Detector

The pyroelectric detector is most popular and widely used for many FTIR applications because of its good detection limit, fast response and affordability (usually less than \$200). If a better sensitivity required, the mercury cadmium telluride (MCT) detector can be adopted. It requires the cooling system to maintain its higher sensitivity. The thermoelectrical cooling can be used in compact applications, or liquid nitrogen cooling in applications of the further higher precision.

1.3.4. Laser interferometer

The laser interferometer takes a very closely coordinated control and feedback mechanism to assist the acquisition of a decent IR interferogram. The apparent solution is to have a perfect motion stage which can move the mirror at a constant known speed. In practice even an expensive optical motion stage can not move at an absolute constant speed nor can the speed be exactly as specified. A more practical and reliable solution is the widely adopted double-interferometer design in which a laser interference signal is also observed. The laser interferometer share the same moving mirror as the IR interferometer.

The theoretical pattern of the laser interferometer is a cosine curve when the mirror is moving at a constant speed. By sampling at every peak and valley or the half transition point the of the cosine wave the IR signal is guaranteed to be sampled with a constant displacement of the moving mirror.

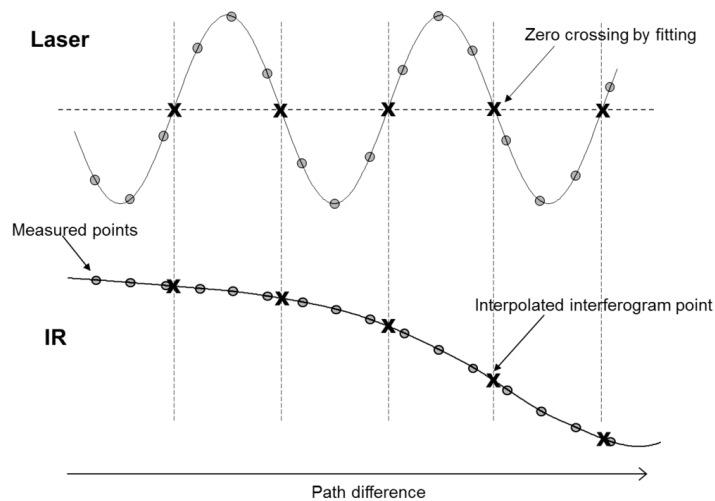


Figure 3. Synchronization of the IR signal and laser signal(Wikipedia)

1.3.5. Sample handling

Gas and liquid samples are generally easy to be handled because they are usually transparent for IR. As for solid samples there are generally three preparation techniques in FTIR: KBr pellet, ATR (attenuated total reflectance) and DRIFT (diffuse total reflectance Fourier transform). Pressing KBr pellet is the most conventional method. It is time-consuming and troublesome. Besides the quality of the KBr pellet affects the base line of the IR spectrum, showing less repeatability and comparability between similar tests. ATR is the most popular FTIR accessory now because of its convenience. The solid sample can be directly placed at the ATR optical window and be pressed for good contact. Some ATR accessories have pressure gauge so that the pressure of the sample on the ATR surface can be controlled to improve the repeatability. However, the quantification of solid samples with ATR is not possible. DRIFT requires no sample preparation. To achieve this there are two parabolic mirrors, one focusing the incident IR beam on the sample surface and the other collecting the diffused reflectance for the detector. The DRIFT technique was chosen as the sample handling method in part of this research to achieve in-situ analysis. There are both advantages of disadvantages using the DRIFT.

The disadvantage of DRIFT is that the IR spectrum baseline is hard to control. A pure KBr sample pellet can be used to acquire the background spectrum. For the ATR the

ATR window is cleaned to acquire a background spectrum. For DRIFT KBr power is used as the background spectrum. Due to many external factors like the difference of the particle size and other surface geometry properties, the baseline of the IR spectrum handled by DRIFT is usually not on 100% (transmittance). The IR spectrum acquired by DRIFT is usually less clear than that acquired by ATR and could be worse than by KBr pellet. Meanwhile DRIFT also shows the least repeatability of the same sample.

At the same time there are many incomparable advantages of DRIFT. First there is no direct contact of the sample with any optical parts or chemical surroundings. This is a great advantage for reaction manipulation. The sample can be heated to more than 1000 °C with no damage to or have chemical interference from surroundings. Non-contact also brings mass measurement possible which is very important in the TG-FTIR project. The reaction control made DRIFT perfect for in-situ analysis. When IR spectrum is acquired in-situ, the best repeatability is achieved because any external factors are the same between the acquirement of all spectra. This feature has great potential for accurate quantitative analysis.

1.4. Data acquisition and instrument control with LabVIEW

LabVIEW is short for Laboratory Virtual Instrument Engineering Workbench, provided by National Instrument. It is a system-design platform and development environment. It is widely used in data acquisition, instrument control and industrial automation. Unlike most programming languages like C/C++ and Java which are designed for developing applications for general PC and internet applications, LabVIEW is designed to provide a link between the virtual world and the physical world. With the

hardware and drivers from NI, it is easy to perform basic measurements like the voltage as well as set an output at a certain voltage, communication through serial port, GPIB, Ethernet etc.

Here are some frequently used terms of a LabVIEW system.

DAQ

DAQ is the abbreviation refers to the data acquisition hardware. The most common DAQ has a USB port to communicate with the PC, a few channels that you can use to measure signals. The most basic type of signal is voltage. Most detectors and sensors reflect their measurement in voltages directly or through an amplifier. There are also DAQs designed for measuring current, capacitance, thermocouple etc. The resolution and maximum sampling rate can also vary by the product quality and levels.

The DAQ is recognized by the PC through the NI MAX driver collection. Once a DAQ is appropriately installed and show up in the NI MAX, it is ready to be used in a LabVIEW program.

VI

All subroutines of a LabVIEW program is call virtual instrument (VI). A VI is made up with a front panel, a block diagram and a connector panel. The front panel can be the user interface with buttons and controls for input and indicators and graphs for output.

Most of the time it is only a collection of inputs and outputs that only the developer will see it. The block diagram is made up with icons, structures and wires etc. It is the code of the VI in graphics. In a proper programming style, the data always flows from left to right, top to bottom along the wires. A block diagram node executes when it receives all required inputs. When a node executes, it produces output data and passes the data to the next node in the data flow path. The movement of data through the nodes determines the execution order of the VIs and functions on the block diagram. This is the basic idea of understanding and reading a LabVIEW code.

While loop

A while loop is a structure in a block diagram. It keeps repeating the code inside until it is set to stop. Many applications are required to run continuously that the while loop is usually used as the control structures. It is very common that a simple application is made up with one while loop and the application is made complicated and more functional by adding more while loops. In the two projects of this thesis, many applications adopted more than two while loops (hereinafter called loop).

Action engine

Action engine is a design pattern. An action engine can be treated as a multifunctional sub VI. By putting in different action parameters the action engine will do different work. An action engine is also called a functional global variable. Holding and protecting a

variable is what made it different from a case structure. The variable is usually a resource that can not be shared, a measurement channel or communication port eg.

State machine

A state machine is a design pattern usually used in programming for the main VI. The different states are like the procedures of a task and the sequence may vary according to external situation. The external factor can be examined when deciding the next state. The states can also be queued which allows control from another loop. This is used in the FTIR project main VI because the loop controlling the motion as to work together with the loop of signal reading.

2 FTIR INSTRUMENTATION PROJECT

To fully understand details of the working principle of a FTIR spectrometer, a FTIR was designed and built. The will allow customized FTIR systems to be integrated with many kinds of chemical reactors for the acquisition of the in-situ spectra signal for better understanding of the reaction process. The commercially available bench top FTIR are restricted in those applications because the hardware are fixed and the software usually does not provide application interface for external command.

The soul of FTIR is FT (Fourier transform). To establish the working principle, system design and selection of some key parameters, FT is first explained and the

computational method is explored. A simulation program is developed to generate the signal of the IR detector so as to test the FT processing code. A further simulation introduced unstable motion of the Michelson interferometer moving mirror. These simulations brought up some crucial issue and provided guidance to selection of some crucial parameters like the sampling rate.

Like the development of every modern instruments the work includes both the hardware setup and software development.

2.1 Fourier transform and data processing

2.1.1 Fourier transform

The Fourier Transform (FT) is a powerful tool for signal processing. Almost any imaginable signal can be broken down into a combination of simple waves. This allows for signal analysis, smoothing or filtering. FT can also be used for solving certain differential equations.

A general function $f(x)$ that is periodic on a finite interval $0 < x < L$ can be written as a Fourier series:

$$f(x) = \sum_{k=0}^{\infty} \alpha_k \cos\left(\frac{2\pi kx}{L}\right) + \sum_{k=1}^{\infty} \beta_k \sin\left(\frac{2\pi kx}{L}\right) \quad (1)$$

Use the exponential form of trigonometric functions and rearrange:

$$f(x) = \sum_{k=-\infty}^{\infty} \gamma_k \exp\left(i \frac{2\pi kx}{L}\right) \quad (2)$$

The sum runs in the range of minus infinity to infinity and the coefficients are give by

if $k < 0$

if $k = 0$

if $k > 0$

$$\gamma_k = \frac{1}{2}(\alpha_{-k} + i\beta_{-k})$$

$$\gamma_k = \alpha_0$$

$$\gamma_k = \frac{1}{2}(\alpha_k - i\beta_k) \quad (3)$$

When the coefficients γ_k is known the original function $f(x)$ can be reconstructed. The orthogonality of the complex exponential on the interval 0 to L can be used to find the coefficients and the following expression can be obtained

$$\gamma_k = \frac{1}{L} \int_0^L f(x) \exp\left(-i \frac{2\pi kx}{L}\right) dx \quad (4)$$

2.1.2 Discrete Fourier transform computation and programming

To solve for the coefficients in Eq. (4) the integrals need to be evaluated. In numeric computation there are several common ways to evaluate integrals: the trapezoidal rule, the Simpson's rule and Gaussian quadrature. Among them the trapezoidal rule has the

least accuracy when using the same computation load. But the signal or function that the Fourier transform is dealing with in this case is not a well behaved one. This makes the trapezoidal rule the most reliable choice. The accuracy can be made up by using more slices(adding computation load) when dividing the integration area.

To evaluate the integral with trapezoidal rules one can use N slices each of width $h=L/N$,

$$\gamma_k = \frac{1}{L} \frac{L}{N} \left[\frac{1}{2} f(0) + \frac{1}{2} f(L) + \sum_{n=1}^{N-1} f(x_n) \exp\left(-i \frac{2\pi k x_n}{L}\right) \right] \quad (5)$$

Since f is periodic, $f(0)=f(L)$. In a real data, the $f(x)$ is known(one signal point) for the sample point x_n so as to define $y_n=f(x_n)$. Eq. (5) can be simplified to be:

$$\gamma_k = \frac{1}{N} \sum_{n=1}^{N-1} y_n \exp\left(-i \frac{2\pi k n}{N}\right) \quad (6)$$

Eq. (6) is the expression for discrete Fourier transform(DFT). The inputs are the sample points and sample number and it is clear enough to be programmatic described. The value of DFT is often referred to as the Fourier transform coefficients c_k despite the fact that they are N times larger than the true coefficients,

$$c_k = N\gamma_k = \sum_{n=1}^{N-1} y_n \exp\left(-i \frac{2\pi k n}{N}\right) \quad (7)$$

Eq. (7) is the final expression for programming. The following piece of code written in Python demonstrated how to do Fourier transform with Eq. (7) .

```

def dft(y):
    N=len(y)
    c=zeros(N//2+1,complex)
    for k in range(N//2+1):
        for n in range(N):
            c[k]+=y[n]*exp(-2j*k*pi*n/N)
    return c

y=loadtxt("Interferogram simple.txt",float)
figure(0)
plot(y)
title("Time Domain")

c=dft(y)
figure(1)
plot(abs(c))
show()

```

The first part of the code is the function description of discrete Fourier transform. A data array containing the discrete signal sample points is taken as the input parameter of the “dft()” function. An array “c” is created to store the FT coefficients. The sample number is acquired by the array length. Every FT coefficient is calculated based on all data points, achieved by two “for loops”. In the second part signal data is read from a text file Interferogram sample.txt and plotted. In the last part the DFT function is called

with the time domain data as input, and the output of a frequency domain array is returned and plotted.

2.1.3 Simulation and FT with LabVIEW

It is necessary to test the accuracy and performance of the FT algorithm and computation code developed above to ensure the reliability of the software developed based on that. To do this the interference output of the IR interferometer is simulated to generate the signal that the IR detector is supposed to provide.

Infrared is inherently an electromagnetic wave. Like any electromagnetic wave, let a beam of single wavelength enter a Michelson interferometer, move one of the mirrors at constant speed, then plot the total energy of the output wave versus time, the result would be a cosine wave (hereinafter referred to as modulated wave). The frequency of this modulated wave is in linear proportion with the frequency of the input electromagnetic wave and the mirror speed (hereinafter referred to as modulated frequency). If the light source is not of single wavelength but a broadband source, the energy of all wavelengths will be added together and the outcome will be a superposition of all the modulated waves. This superimposed wave is the interferogram that the control system is supposed to acquire from the IR detector.

To simulate the interferogram the virtual FTIR was defined to work with certain parameters. The Michelson interferometer was moving its moving mirror at a speed of v . The total distance that the mirror will move during a scan is d . The signal of the IR detector will have a sampling rate of f_s . The modulated frequency of a certain wavelength is f' .

Table 1.

Simulation parameters	Expression	Description
Sampling rate	$f_s \cdot d/v$	How many points to generate
Amplitude	given	The amplitude of the sine wave
Frequency	f'/f_s	How many cycles one point covers

Wavenumber(number of cycles in 1cm) is commonly used instead of frequency or wavelength in IR region.

$$W_n = 10000 / \lambda \quad (8)$$

where λ is in micrometers. Thus the modulation frequency f' can also be written as

$$f' = 100v \cdot wn \quad (9)$$

where wn is wavenumber in cm^{-1} and v is in meters.

The Sine Wave VI (Fig. 4) provided by the LabVIEW development environment is used to generate the modulated waves. Among its input parameters, the frequency and samples are calculated from Table 1. The amplitude is imported from a sample.txt file which is a real IR spectrum. The phase is left default.

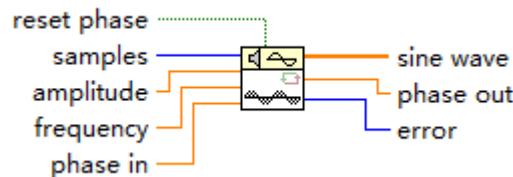


Figure 4. Sine Wave VI

The Signal Generator VI (Fig. 5) is created to generate the interferogram. For each run of the Signal Generation Loop only one modulated wave in accordance with a

wavenumber is created. All the modulated waves have the same number of samples and are added together to create a superimposed wave, the interferogram. The loop will stop when the specified wavenumber is reached.

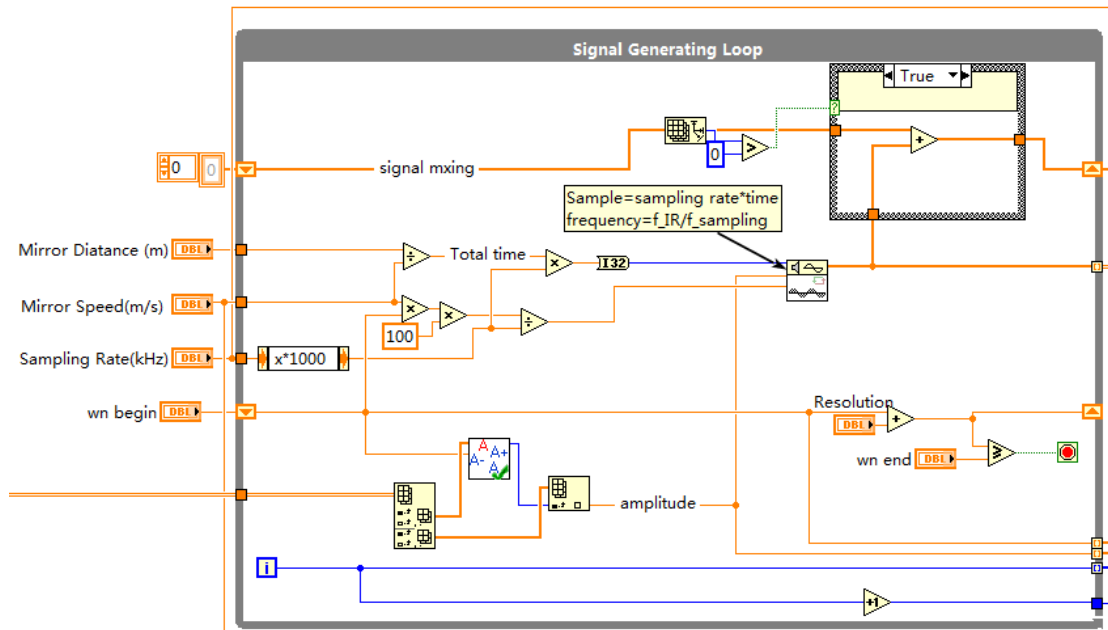


Figure 5. Signal Generation Loop.

After the interferogram is generated by the main loop it is built into a waveform by introducing the time increment. The time increment is the reciprocal of the sampling frequency f_s . Then the FFT Power Spectrum VI is used to perform the Fourier transform to get the frequency domain data, the spectrum. The for loop is used to construct the x axis of the frequency array. The frequency is further converted into wavenumber with Eq. (9).

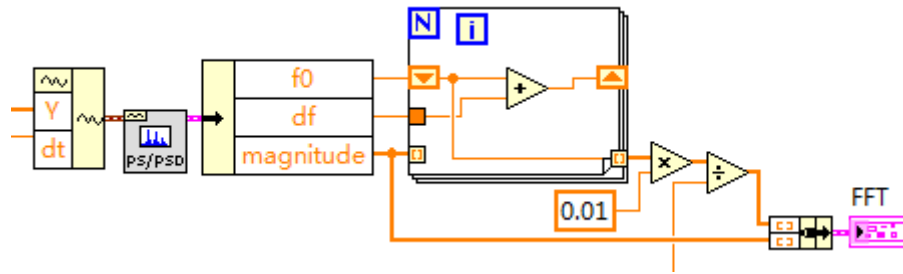


Figure 6. LabVIEW code for Fourier transform

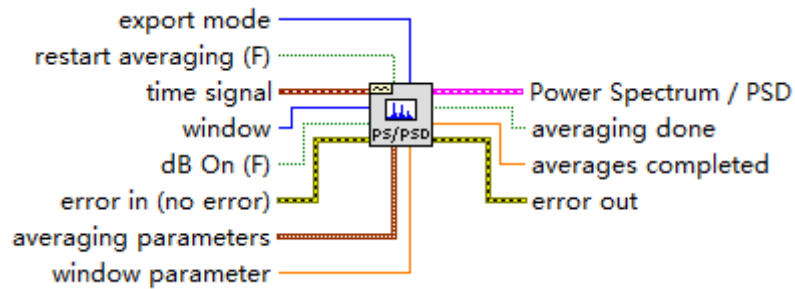


Figure 7. FFT Power Spectrum VI

A simulation was run with some typical operation parameters (Table 2) of a FTIR.

Table 2. Simulation parameters

Wavelength range	4000-400 cm^{-1}
Mirror speed	0.001 m/s
Mirror distance	0.004 m
Sampling rate	10 kHz
Resolution	4 cm^{-1}

The amplitude is introduced from a carbon dioxide IR spectrum shown in Fig 8.

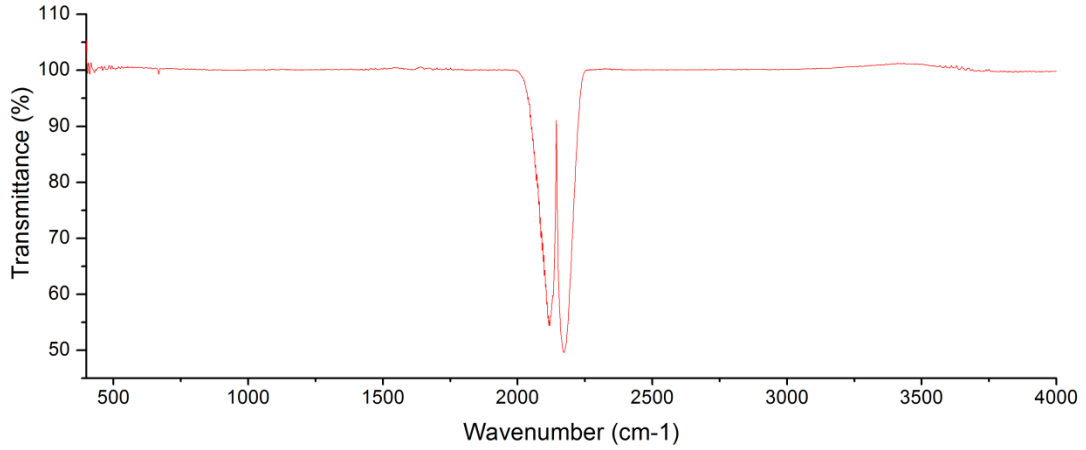


Figure 8. Amplitude data for simulation.

Fig. 9 shows a snippet of the modulated waves generated before they are mixed. Each wave has a different frequency and amplitude with the others. This snippet is taken from where the valley of the CO IR spectrum is. In other regions all waves should have the close amplitude since the amplitude data shows a flat curve in most of its range.

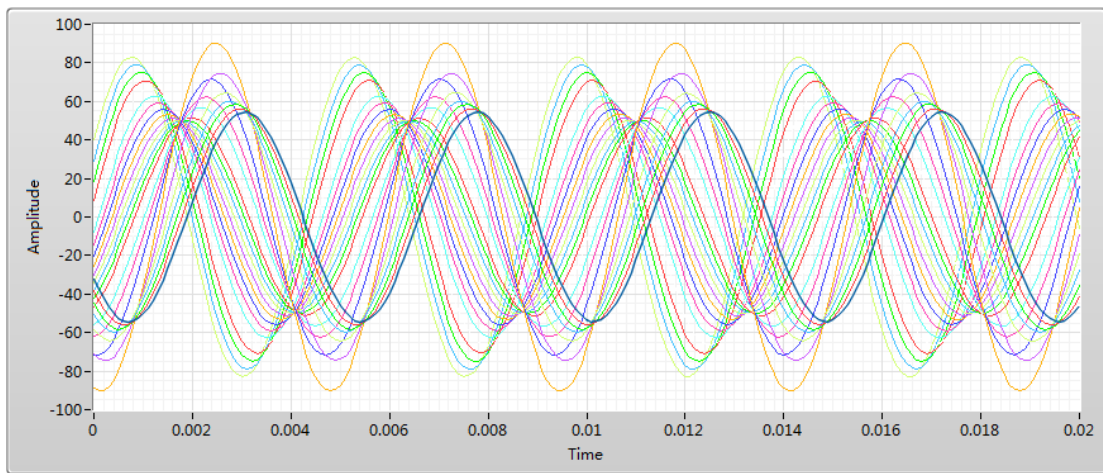


Figure 9. Collection of some of the modulated waves

Fig. 10 shows the interferogram generated. The maximum peak and valley in the center indicates the situation when the two arms of the Michelson interferometer are equal in distance which is also called zero retardation point.

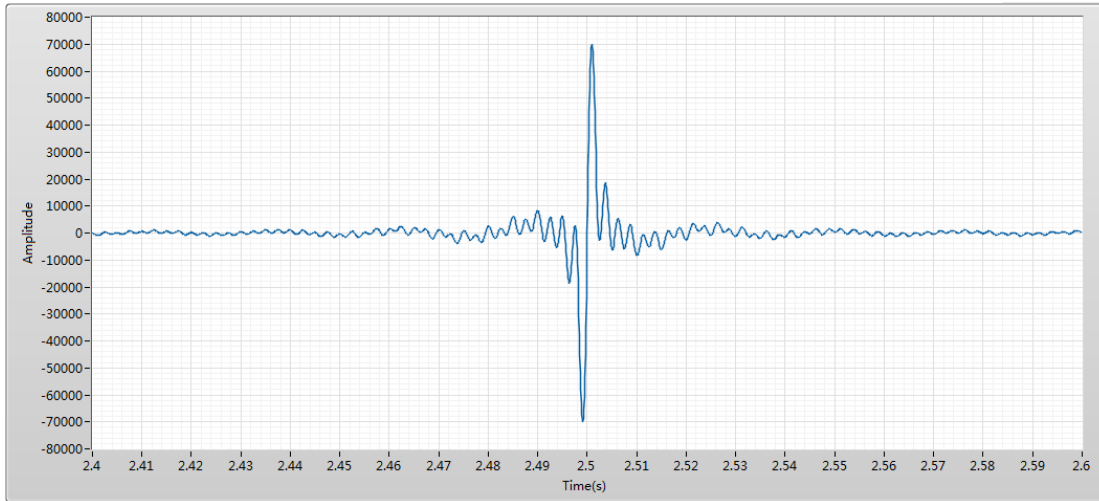


Figure 10. Interferogram simulated

The Python code for FT is tested with the interferogram generated and the result is shown in Fig. 11. Since time is not introduced in this code, the x axis only represents of the index of the FT coefficients.

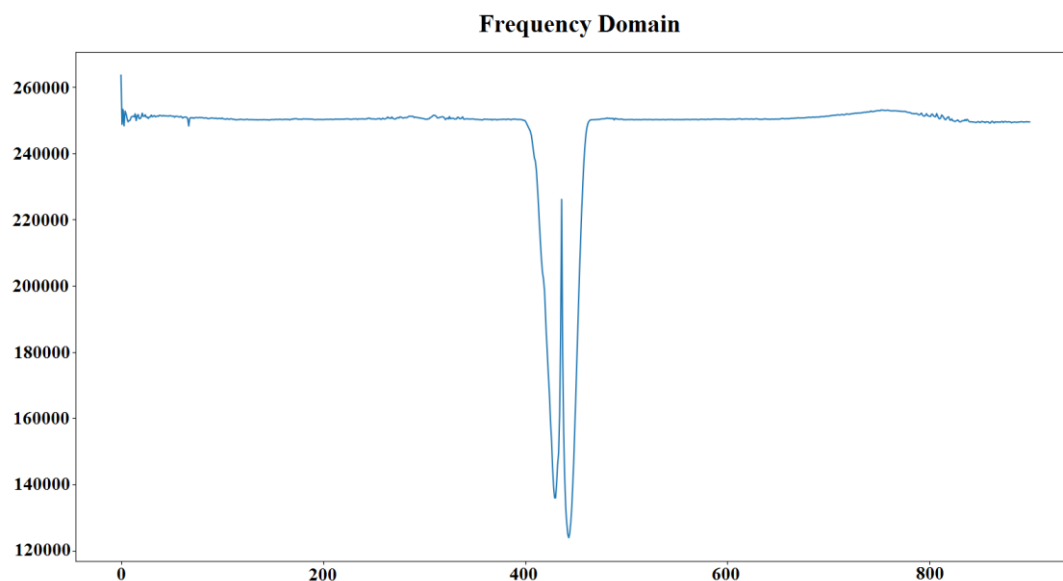


Figure 11. The FT result of the Python code

The FT result of the LabVIEW code is shown in Fig. 12. The curve resembles the original data in Fig. 8 in great detail. The difference of values in the y axis can be ignored since only the transmittance or absorbance is needed and both of which are obtained by comparing with the blank spectrum.

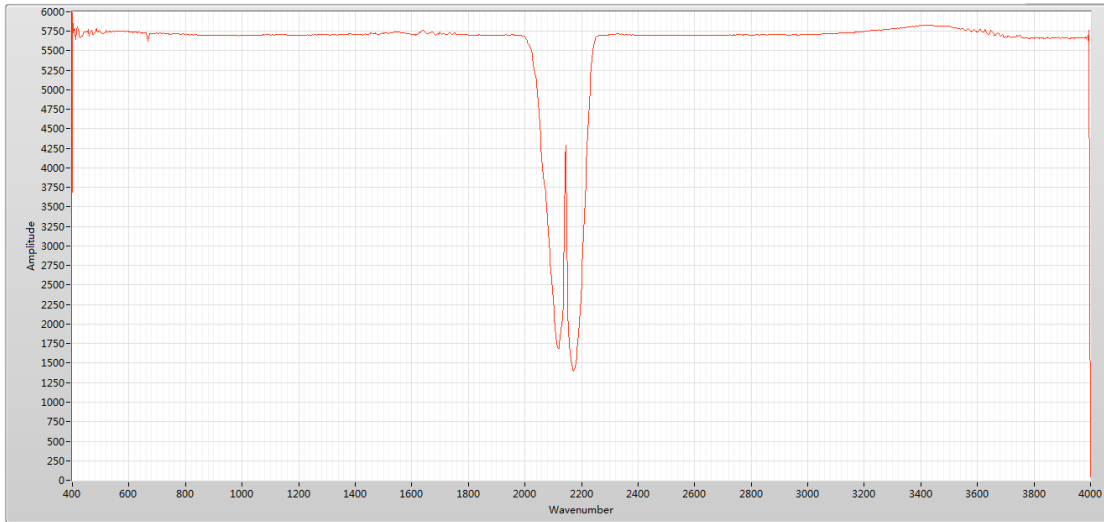


Figure 12. Fourier transform result of the LabVIEW code

In the simulation above a sampling rate of 10kHz was adopted. Generally the higher sampling rate is the closer the data acquired is to the real signal. But higher sampling rate means more sample points and more computational load and time. It is important to find an optimum sampling rate.

When the sampling rate is lowered to 1 kHz, the modulated waves and the corresponding interferogram looks very rough but the Fourier transform still gets very high quality result.

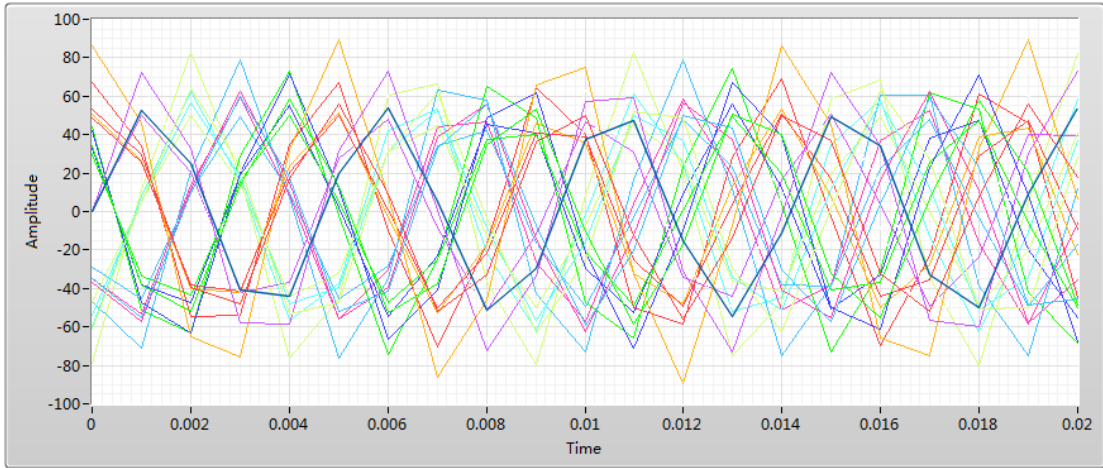


Figure 13. Collection of modulated waves(sampling rate 1 kHz)

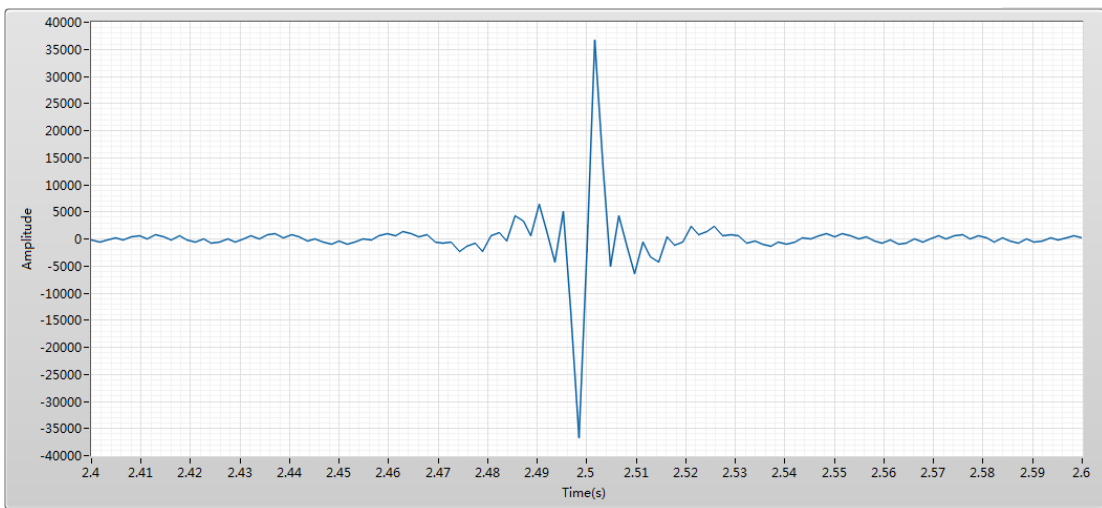


Figure 14. Interferogram generated (sampling rate at 1 kHz)

If the sampling rate is lowered even more, etc. 0.62kHz, the sine waves will look even tougher. Some of them has lost the shape of a sine curve. The interferogram also worsened. The Fourier transform result becomes incorrect. As shown in Fig. 15, the first half of the curve looks still good, detail well kept but for wavenumber beyond around 2200cm^{-1} , the curve suddenly all dropped to zero. This is attributed to the nature of FT.

Every FT coefficient is evaluated by looking at every sample point in the time domain data. If the wave of corresponding frequency exist, the magnitude of that wave is reflected to the FT coefficient. When the sampling rate is too low that some wave of higher frequencies can not be detected and are not kept in the time domain data.

The frequency of a modulated wave depends on the IR wavelength as well we the mirror speed. In this case, the modulated frequencies range from 40 to 400Hz when the mirror moving at 0.001m/s. In data acquisition, the sampling rate usually has to be at least twice of the signal to identify the frequency of the wave. With a sampling rate of 0.62k, it meets the minimum requirement of the 310Hz wave and below. In Fig. 15, the curve crushes at wavenumber 2200cm^{-1} which corresponds to the sine wave frequency of 220Hz. That means the actual sampling rate needed is close to but more than two times of the signal frequency. On the other hand, as long as the sampling rate is high enough to make effective detection of the high frequency part of the signal, a full frequency domain result will be obtained and increasing the sampling rate based on this will not improve the quality of the FT result too much. In this case the simulation shows that 0.8kHz is the minimum requirement. Since most FTIR use the same range of wavenumber, the only variable is the mirror speed with which the sampling rate should be in positive proportional correlation. For example if the mirror speed is 0.002m/s, the minimum sampling rate should be 1.6kHz.

But there is some merits in using higher sampling frequency. The number of FT coefficients is half the number of sample points. That means the resolution is improved directly by increasing the number of sample points. There are two ways of getting more sample points: higher sampling and longer scanning distance.

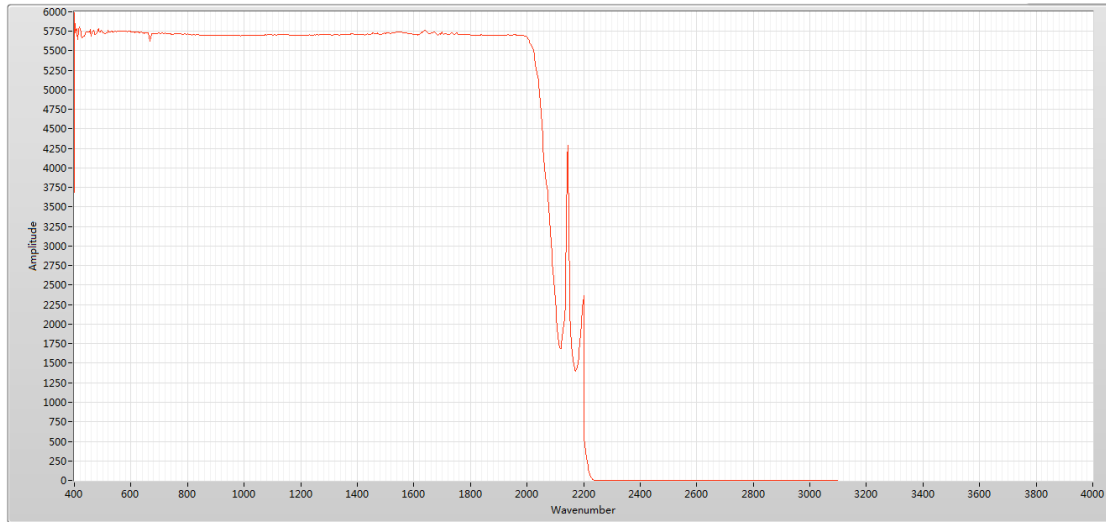


Figure 15. FT result with a sampling rate of 0.62kHz

2.1.4 Simulation with unstable scanning speed

In the simulation above, The mirror speed was assumed to be exactly as stated. But in the actual situation it is very hard to make the motion stage move at a constant speed. The mirror speed directly affect the modulated frequency, stretching or compressing the interferogram every time the mirror moves at a speed different with what it is set to be. The FT result from this interferogram acquired will be inaccurate or totally wrong.

The solution to unsteady motion is to use a laser accompanied with a Michelson interferometer. In most design the laser share interferometer with the IR beam. The most commonly used laser is a 635nm laser. If the motion stage moves at a constant speed, the detector of the laser will get a perfect cosine wave. If not, this sine wave will be stretched or compressed when the unsteadiness happens. Despite the sine wave being distorted, when peak turn into a valley, it is known that the motion stage has moved half the

wavelength of the laser wave. By taking a sample of the IR detector when a valley, peak or a half transition point is captured on the laser detector, one can make sure that the sample points of the IR detector is taken evenly in terms of the mirror moving distance.

In practice it is easier to sample both the laser and IR detector at relatively high rate and choose the appropriate points from the IR data based on the laser data later instead of dynamically analyzing the laser signal.

The Signal Generator with Laser VI (Fig. 16) is created to simulate the IR data together with the laser data with the unsteady motion problem and addressing the solution with laser referencing system. This VI uses the IR data generated by the Signal Generating VI and create a perfect cosine wave with the same number of sample points as the IR data as the laser data. So far both the IR data and laser data refers to the motion-steady situation. Fig. 16 shows the for loop in the Signal Generator with Laser VI. Both the IR data and the laser data are inserted with some middle points in a random style. Every time this program is ran the stretch or compress will appear at different time to different extent. Fig. 17 shows the snippet of the IR signal and the laser data generated for unsteady-motion situation.

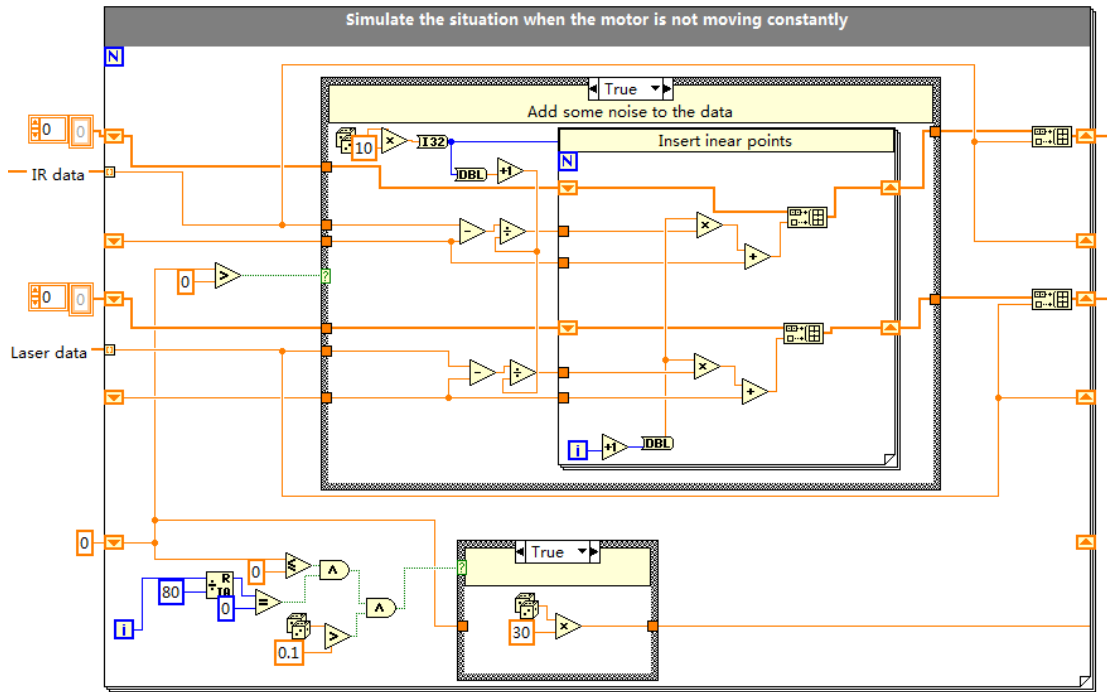


Figure 16. Main loop for adding stretching and compression points into the IR and laser signal.

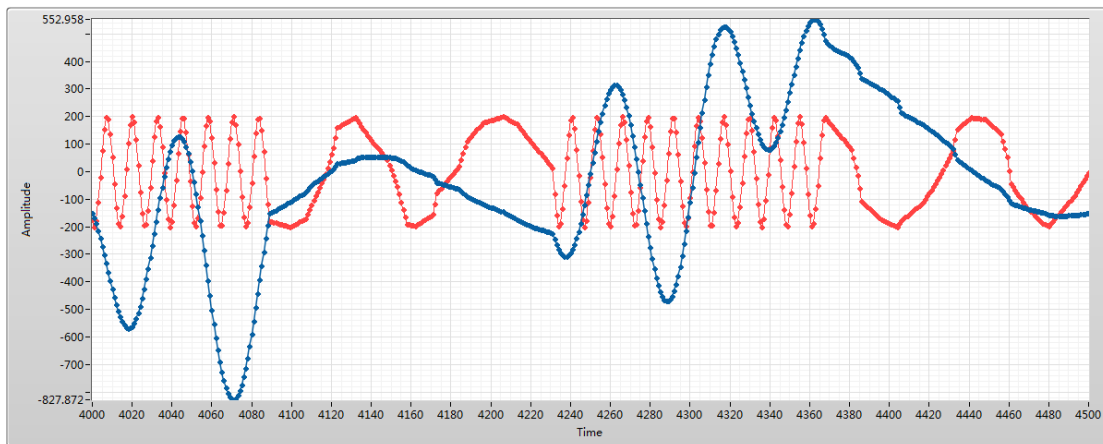


Figure 17. IR and laser data for unsteady scanning. Red line is laser signal and blue line is IR signal.

Fig. 18 shows the FT result based on this unsteady-motion IR interferogram. The CO spectrum is totally lost.

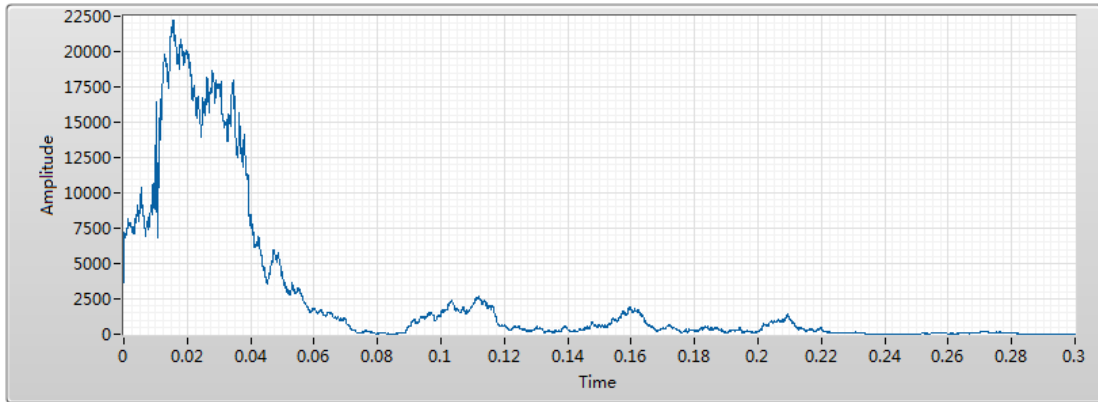


Figure 18. FT result with bad interferogram

2.1.5 Synchronization and test

When the IR signal and laser signal are both acquired they need to be synchronized before FT processing. As shown in Fig. 19 the unsteadiness has impact on the signal of both IR and laser at the exactly same moments. This synchronization process is basically about finding the effective data points in the IR data acquired.

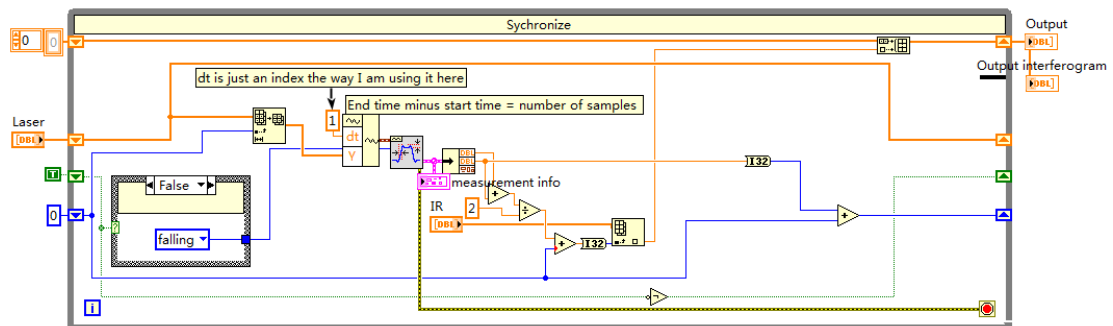


Figure 19. Synchronize loop

The basic working principle of the synchronization is to detect the transition in the laser signal. The Transition Measurement VI (Fig. 20) is used to find the first transition of the given signal. The IR sample points at the middle of a transition of the laser signal are chosen. The measured part of the signal is cut before the next run of the loop, and the transition measurement will start from the end of the last transition. Using the sample points at the valley or peak is also feasible.

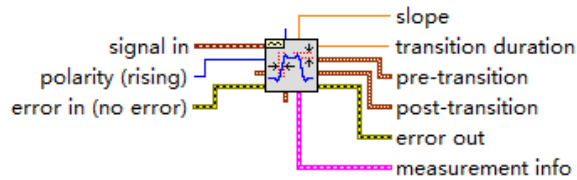


Figure 20. Transition Measurement VI.

Fig. 21 shows the interferogram simulated for a unsteady-motion scan. By synchronization about 70% of the data points are discarded and the interferogram in Fig. 22 can be obtained.

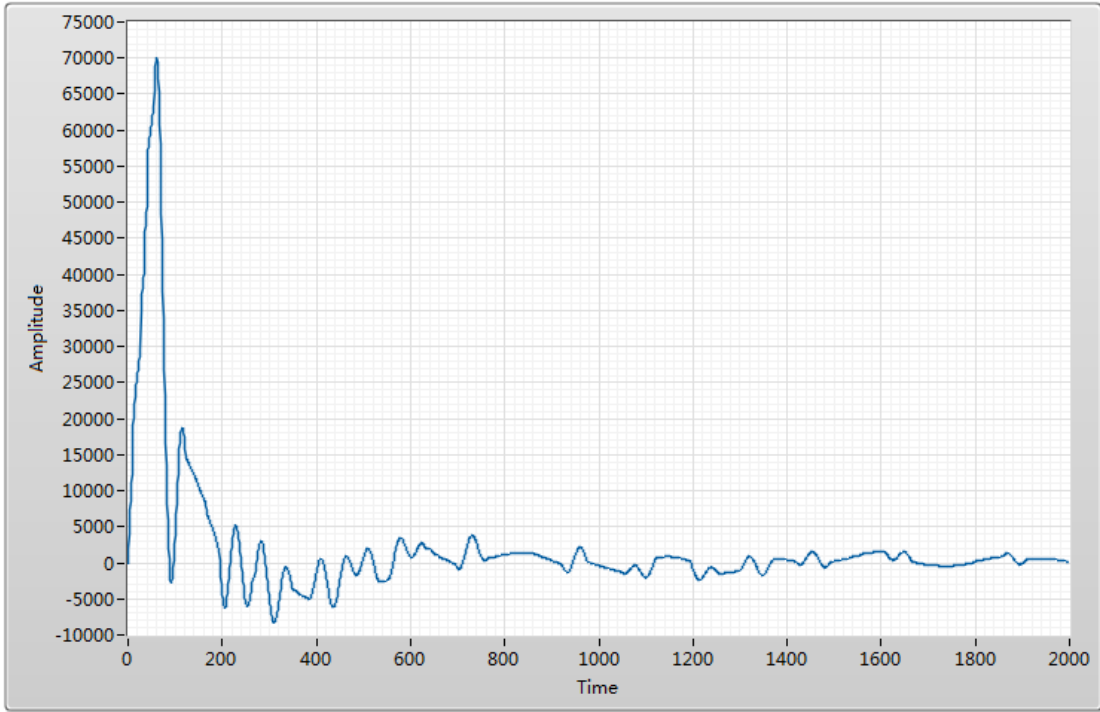


Figure 21. Interferogram before synchronization process

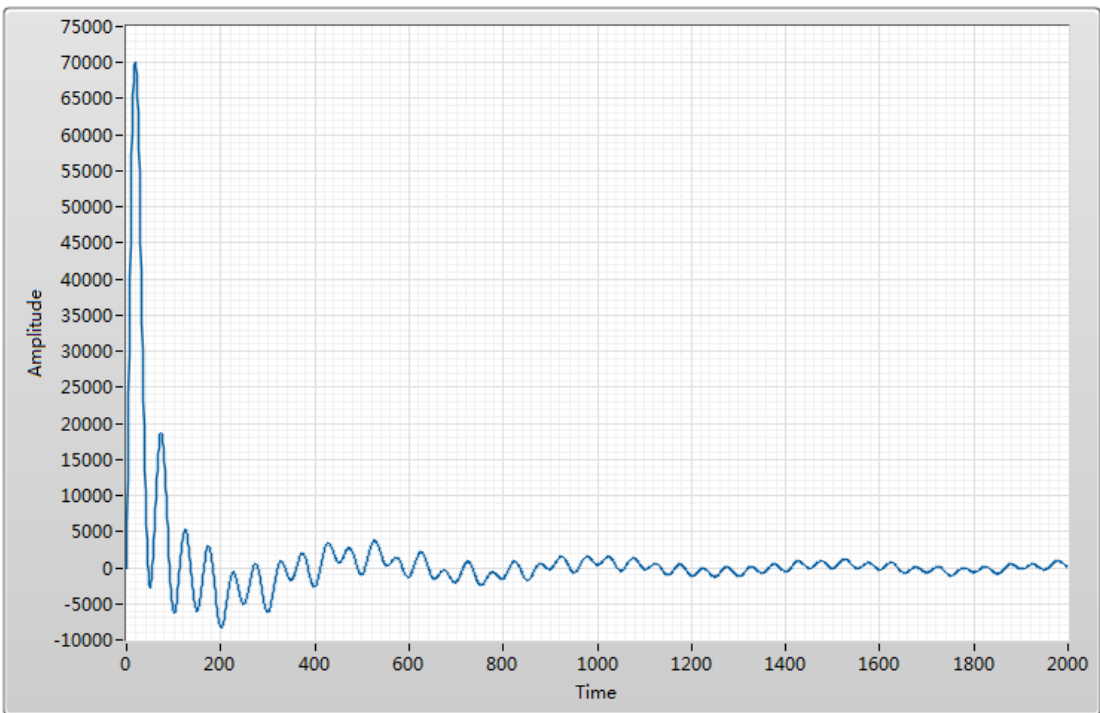


Figure 22. Interferogram after synchronization process

Fig. 23 is the FT result of the synchronized interferogram. The CO spectrum is fully recovered, demonstrating the effectiveness of the laser referencing system and Synchronization VI.

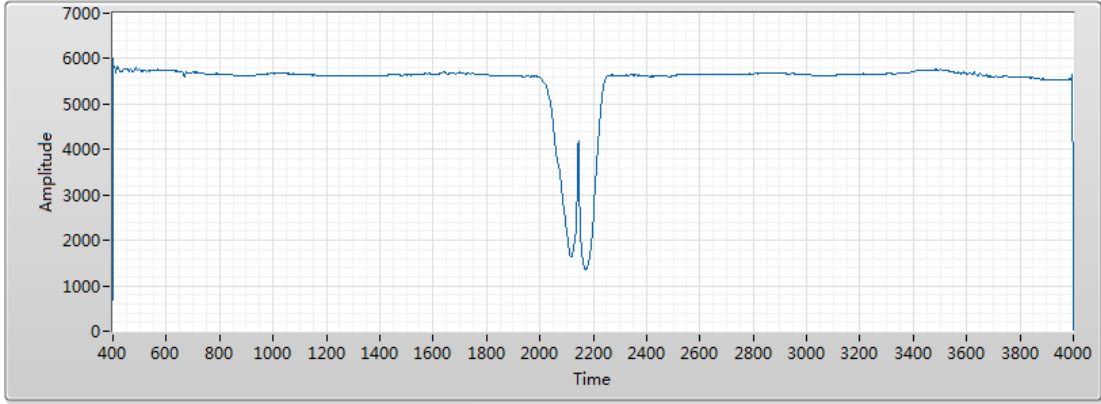


Figure 23. FT result of the synchronized interferogram

It is very important that when the motion is not stable the sampling rate of the IR and laser detector can not be set as low as the minimum rate as is discussed at the end of Chap. 2.1.3. There has to be enough points to plot the modulated wave of the laser signal so that the transition can be found accurately. Here is a simple method to calculate the rough sampling rate needed.

$$f_s = \frac{vn}{\lambda} \times 10^9 \quad (10)$$

Where f_s is the sampling rate, v is the mirror speed(m/s), λ is the laser wavelength in nm, n is the number of point to cover one cycle of the laser modulated wave. Based on Eq. (10) the minimum sampling rate is 31.4kHz. The test of the Synchronize VI showed

that the synchronization becomes very good at over 40kHz. Higher rate does improve the result very much but take long time for computation.

2.2 Hardware setup

The hardware setup of the current FTIR was initialized using components of the outdated PerkinElmer FTIR. This platform provided a complete wave path from the light source to the detector which is made up of many a few parabolic mirrors and concave mirrors. The light source is also provided. To make the FTIR complete, two Michelson interferometer need to be added. Fig. 24 Shows the layout of the optics of the FTIR with the two Michelson interferometers at the center.

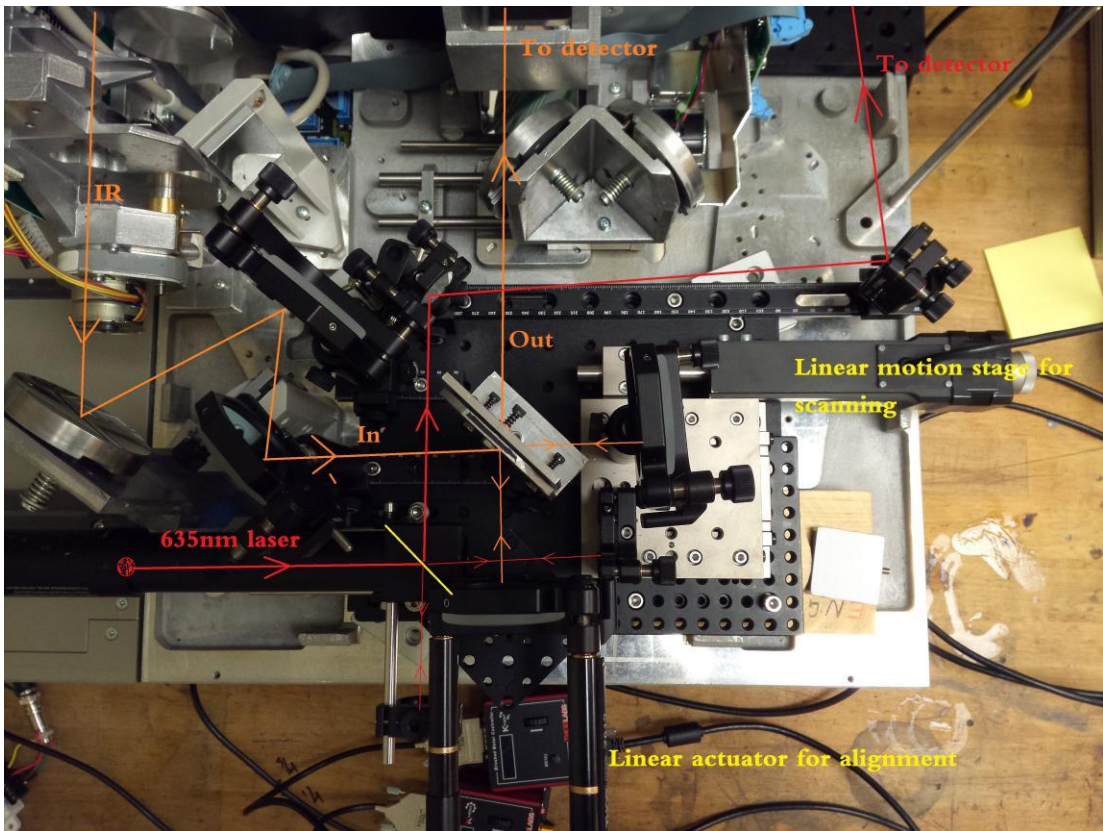


Figure 24. The layout of the FTIR optics. The IR source and two detectors are not included in this scope.

The IR source is a resistance coil heated to 1500 K to 2200 K, producing a continuous radiation close to that of a black body. The maximum radiation intensity was in a range between 1.7 μm to 2 μm . It fall smoothly approaching the longer wavelengths until 1% of its maximum at around 15 μm . The IR wave was firstly collected by an parabolic mirror to form a roughly parallel wave, then passed through two adjustable aperture so that the extra spatial noise can be removed. To guide the IR wave in the desired light path, both normal mirrors and concave mirrors were used, and the concave mirrors guarantees that the IR wave would not expand too much along its transfer within this long light path.

Two DC servo motor actuators mounted the fixed mirror were used alignment of the Michelson interferometer. The DC servo motor actuator has a bidirectional repeatability in distance of less than 1.5 μm . The DC servo actuators ensured the required alignment of IR beam with higher accuracy. The moving mirror is mounted on a high precision motion stage driven by an high precision stepper motor actuator. This moving stage had a bidirectional repeatability in distance of less than 1 μm and a minimum increment movement at 50 nm. It ensured a precise control of the scanning process. The moving mirror of the interferometer for the laser was also located on the same moving stage of the IR interferometer to ensure their same movement.

A high performance pyroelectric detector (LIE-332f#, Fig. 25) purchased from InfraTec is used for IR detection. This detector adopted metal black as the IR absorbing layer and has a very stable response across 1 μm - 25 μm .



Figure 25. Pyroelectric detector

A Junction Field Effect Transmitter(JFET) amplifier is built in the detector. The main advantage of an JFET used for amplification is that it has very high input impedance and low output impedance. The external operation amplification circuit (Fig. 26)was built

with the OPA227 IC(Texas Instrument). The laser signal was detected using a biased photo diode. Both detectors were sampled to a NI DAQ.

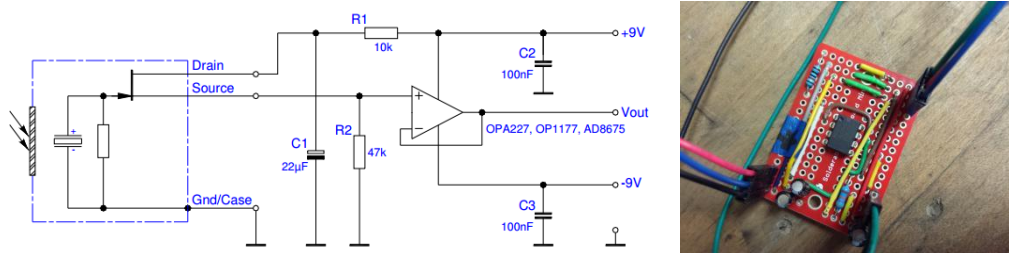


Figure 26. External amplification circuit and diagram

2.3 Software development

There are three motors and two detectors involved in this system. To get an IR spectrum the two detectors has to be sampled simultaneously while moving the moving mirror through a certain distance. The scan may repeat multiple times to obtain one spectrum. This requires highly coordinated control and data acquisition.

The FTIR LabVIEW project (Fig. 27) is developed to make the hardware system function as designed. There is one main VI and eight sub VIs.

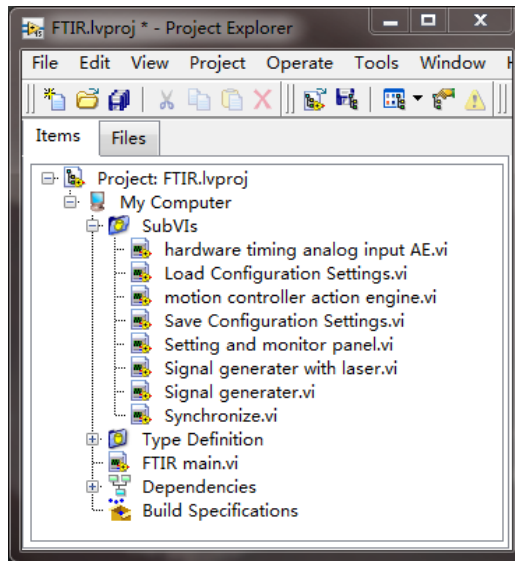


Figure 27. LabVIEW software project FTIR

Table 3. FTIR LabVIEW project VI list

VI	Description
Hardware timing analog input Action Engine	Achieve high frequency sampling of the IR and laser detectors
Load Configuration Settings	Load the settings saved from last running, including physical channels, sampling rate, and settings of the motions stage (start and end positions etc.)
Motion Controller Action Engine	Use ActiveX to control the motion stage
Save Configuration Settings	Save all parameters of the current run
Settings and Monitor Panel	Call a new window to access current settings

Synchronize	Interpret the raw data of IR and laser signal to get the IR interferogram
Signal Generator	Simulate the interferogram of an IR wave of continuous wavelength.
Signal Generator with Laser	Simulate the interferogram of an IR wave of continuous wavelength accompanied with laser signal (to test the synchronize VI).

The FTIR VI has three while loops:

Table 4. FTIR VI structure list

Event Loop	Handle user inputs and operations of the front panel
Main Loop	Execute commands from event loop, call signal loop
Signal Loop	Acquire IR and laser signal

The reason the functional codes can not be placed in the one loop is that during a scan, the main loop will wait on the motion stage moving and the IR and laser signal needs to be acquired at the same time non stop. Using two loops will allow this two task to be executed simultaneously. The event loop keeps the user interface to be active.

The Main loop is a state machine with five states (Table 5)

Table 5. Main Loop state machine states list

States	Description
--------	-------------

Initialize	Home the motion stage, initialized analog input
Obtain Spectrum	1. Move the motion stage and call signal loop to start reading IR and laser signals 2. Process data to get and IR spectrum
Process Data	Get the IR spectrum with IR and laser data
Monitor	Call for monitor state of the Signal Loop
Setting	Open the setting panel, apply setting
Shut Down	Shut down all VIs and ActiveX component, save settings in configuration file, close all loops.

The Read Signal Loop is a queued state machine. It does not have an inter mechanism of working in a series of states but takes external commands of which state to take. The commands usually does not come as a list of things to do in sequence, finishing one after another. Table 6 included all the commands that can be placed in queue by the main loop. This loop works as a independent data hunter. There is only three states in this loop .

Table 6. States of Read Signal Loop

States	Description
Monitor	Display all status: stage position, IR& laser sensor value
Scan	Sample the IR and laser sensor simultaneously and transfer them back to the main loop
Shut Down	Stop the loop

The Obtain Spectrum (Fig. 28) is the most important state of Main Loop. The structure that resembles the film is the sequence structure which will make sure that the code execute in sequence instead of simultaneously. In the first frame, the moving mirror is started to move to a position provided by the Setting VI and the data acquisition is started. In the second frame the mirror is controlled to move back to original point while the data acquisition continuous. In the third frame the data acquisition is stopped and data processing is started. The data will be sent to the Synchronize VI (Fig. 29) and then to the FFT Power Spectrum VI to get the IR spectrum.

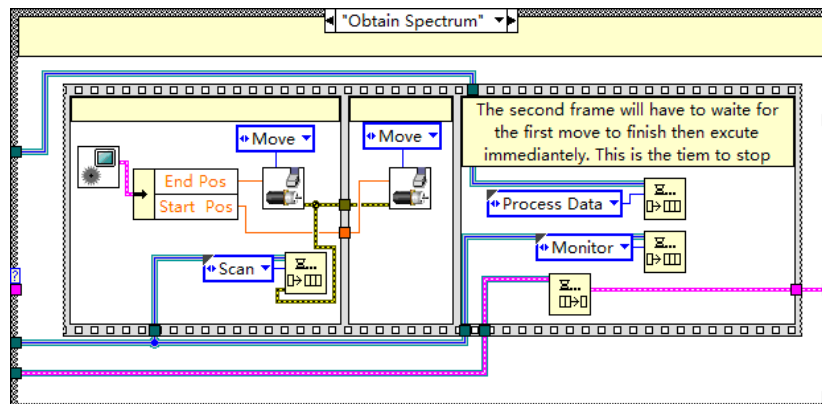


Figure 28. The Obtain Spectrum state of Main Loop



Figure 29. Synchronize VI

The motion stage is controlled via ActiveX. The manufacture of the linear actuator has provided a software called APT which contains the controller driver and an ActiveX interface. The LabVIEW controls the motion stage by communicating with the APT software and the APT software communicates with the motor controller. When an ActiveX component is introduced to the project one can have access to the attribute nodes of the ActiveX component. By writing or reading the attributes the motion stage control is fulfilled. The most frequently called attributes are listed in Table 7:

Table 7. Motion control ActiveX attributes

Attribute name	Description
HWSerialNum	Each device has a unique serial number. Input the serial number unique for each APT device to identify different devices.
StartCtrl	Start the ActiveX control.
MoveHome	Move the actuator to the home position
SetVelParams	Set moving velocity
SetAbsMovePos	Set absolute moving position. If homed, the home will be the zero position.
MoveAbsolute	Start moving the actuator to the position set in <i>SetAbsMovePos</i>
StopProfiled	Stop the actuator immediately

GetPosition	Get the current position
LLGGetStatusBits	Get the status bis of the actuator
StopCtrl	Stop and close the ActiveX control, release the related resources.

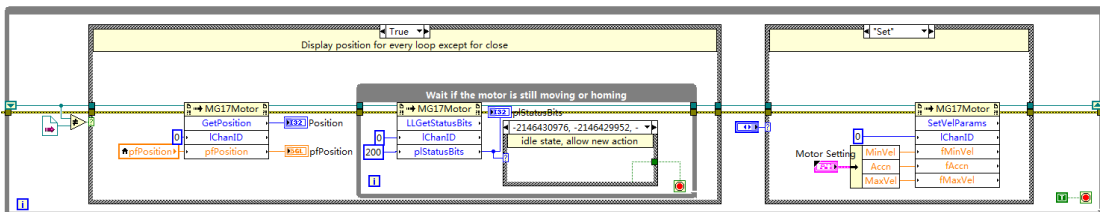


Figure 30. Motor control action engine block diagram

Unlike a piece of LabVIEW code, the ActiveX attribute node does not execute in data flow mode. In LabVIEW a node has to wait for the ones before finished and passed output to it to execute. But when using ActiveX when a attribute after starts to execute, it does not necessarily mean that the one before has finished because the ActiveX is running outside of LabVIEW environment. It could happen that one could be writing to a new moving command to the attribute node while the actuator has not yet reached the destination given by the last command. The motion controller action engine needs to be able to wait if the actuator is still moving before it execute with a new task.

Every time the motor controller action engine executes, instead of going directly into to the case structure where the task is, it uses the LLGGetStatusBits attribute to get the status code of the actuator. If the status code shows that the actuator is not moving then the while loop can stop to allow the program to proceed.

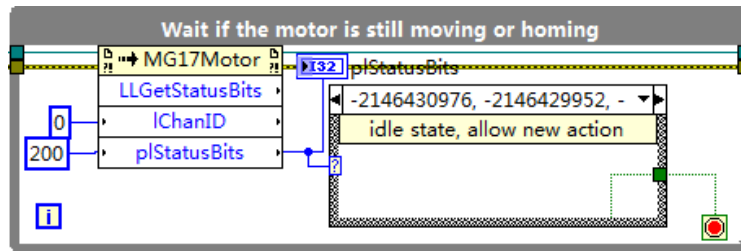


Figure 31. Motor moving status testing code

This feature is even more important when the main loop is in Obtain Spectrum state where the signal reading of IR and laser detector needs to be stopped right after the motor finishes moving.

3 TG-FTIR PROJECT

Two most frequently used tools, TG and FTIR are combined for the purpose of opening the door to more details about kinetics in fuel pyrolysis, combustion and other dynamic behaviors.

DRIFT(diffuse reflectance infrared Fourier transform) is a powerful tool to provide in-situ IR information revealing subtle changes in functional groups as well as semi-quantity information of the sample. TG (thermogravimetry) can provide mass information during the temperature variation of the sample. By combining In-situ FTIR and TG signals the semi-quantity information can be explained with reference dimension of mass and the overall reaction kinetics and is potential to be enhanced to be a precise kinetic parameter on each absorption line in the whole IR spectrum.

3.1 Hardware setup

The main part of a TGA is a micro balance in a sealed furnace. The main unit for a FTIR is a go-through wave path (absorbance chamber, ATR, DRIFT etc.). In the design the micro balance is located at the top of the DRIFT chamber. A metal string hangs down hooking the sample pan from the top through the slit between two parabolic mirrors, one focusing the IR beam onto the sample and the other collecting the diffused reflectance from the sample and lead them to the detector. Underneath the sample pan there is a tube furnace to control the temperatures of the sample. There is a small opening at the top of the furnace which is just enough to allow the sample pan in so that the heat is restricted to sample and does not heat the whole chamber too much.

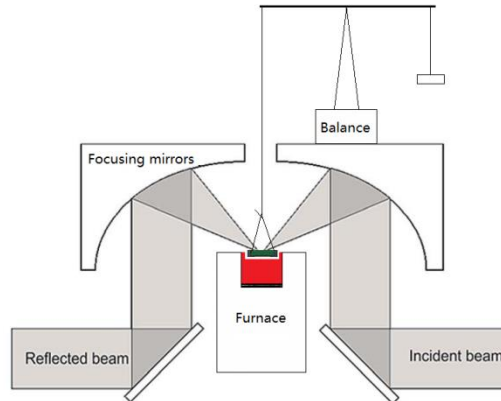


Figure 32. TG-FTIR schematic diagram

The actual set up (Fig. 33) is much more complicated than the basic design. First of all the commercial micro balance is very expensive (cost about \$20,000 with the controller and software) and is not an option. To ensure the readability of less than 1 μg , the

balance of an old TGA 2950 was refitted to the system. Because the balance has to work with the mother board of the TGA, the whole TGA and its communication PC was introduced into this system. The IR spectrum is collected with Spectrum Two(PerkinElmer). The FTIR also has to communicate and being controlled by the original PC with its software. The temperature is measured with a thermocouple which is read with a NI 9213 DAQ. The furnace is powered with a programmatically controlled DC power supply. All data is collected by the main control PC. The balance over the DRIFT chamber is sealed with plastic board chamber to reduce interference of air flow.

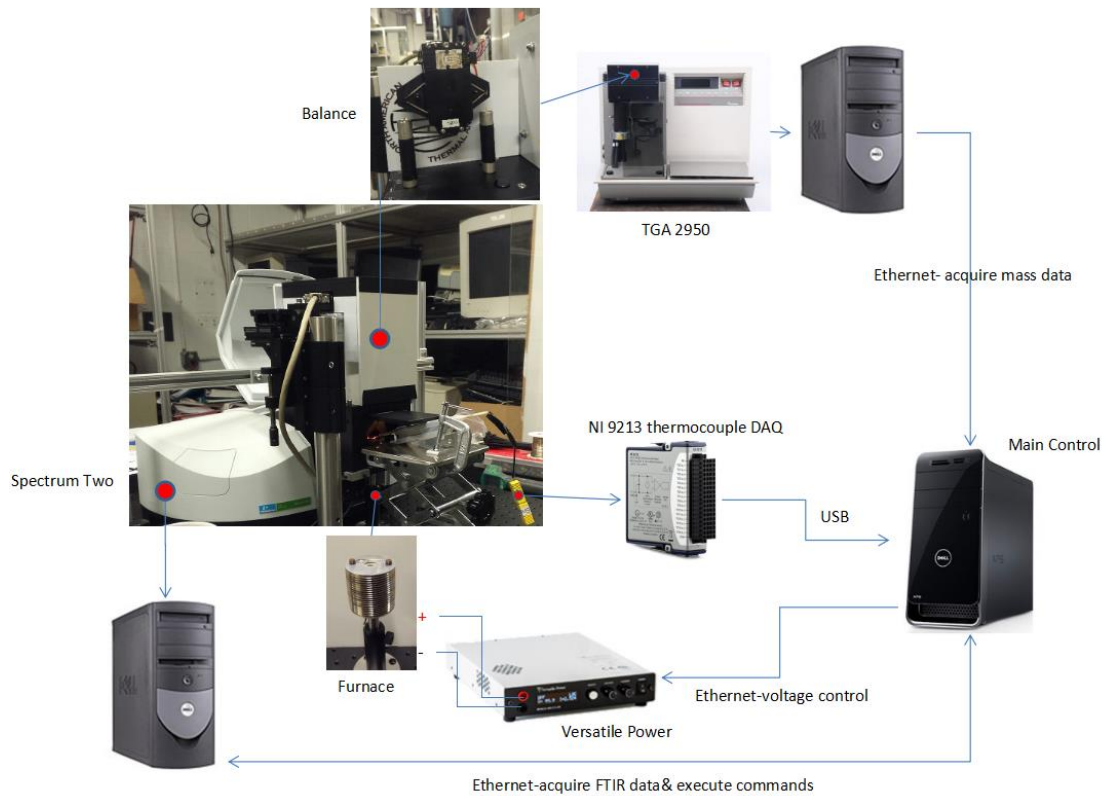


Figure 33. Hardware setup

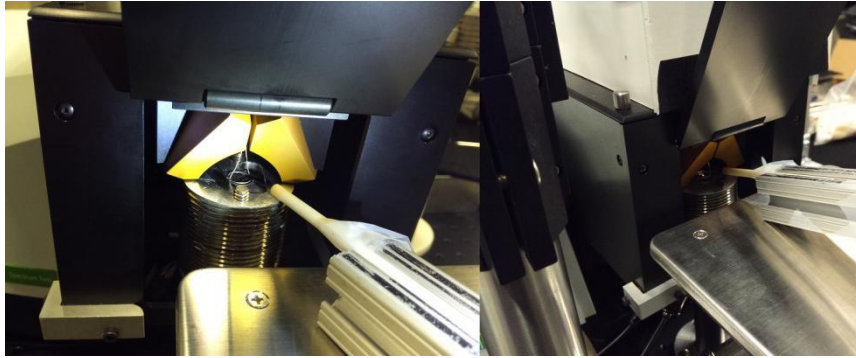


Figure 34. Inside the DRIFT chamber

3.2 Software Development

There are two PCs, one NI DAQ, one power supply that need to be communicated either for data transfer or programmatic control. The TG signal and IR spectrum data are both acquired from software on separate PCs. This requires two separate programs to work with each software to achieve communication with the programs on the main control computer through Ethernet. The power supply is controlled through the Ethernet directly. The NI DAQ communicates with the main control via USB.

The TG-FTIR LabVIEW project package is shown in Fig. 35. There are totally 20 VIs (Table 8) created to achieve all functions and features. Among them there are three most important stand alone VIs that are used as distributed applications: TGA Server, FTIR Server and Main Control. The other VIs are created for specific functions to be used repeatedly for programming efficiency.

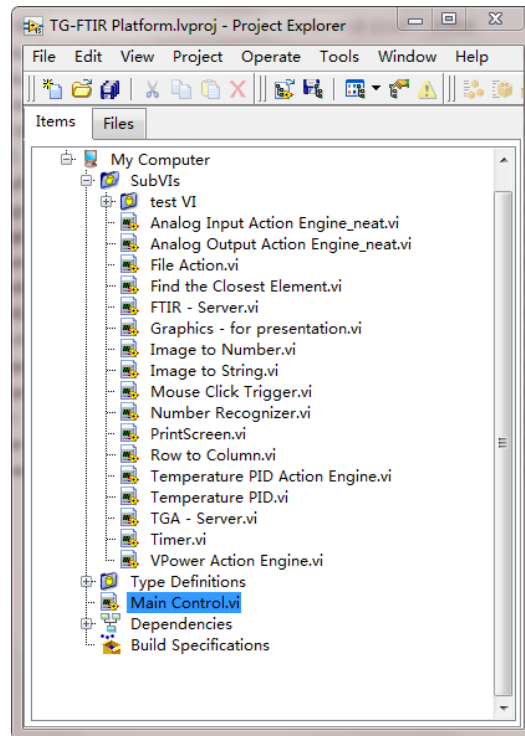


Figure 35. TG-FTIR project list

Table 8. TG-FTIR VIs and descriptions

VI	Description
TGA Server	Read mass data from the TA instrument control software and send it back to the Main Control
FTIR Server	Read the IR spectrum data from the Spectrum software and send it to the Main Control. Execute commands on the Spectrum software from Main Control

Main Control	Control all sub instrument of the system, collect all experiment data and store them in disk
Analog Input Action Engine	Initialize, read from and close an analog data acquisition channel
Analog Output Action Engine	Initialize, write to and close an analog data acquisition channel
File Action	Get current working folder path, create new folder, write data to file
Find the Closest Element	Search an array and find the element which is closest with the reference value
Graphics-for Presentation	Plot the TG curve and IR spectra
Image to Number	Read an image and recognized the number in it
Image to String	Put an image file into a string for transfer
Mouse Click Trigger	Trigger a event equal to a physical click of the mouse
Number Recognizer	Interpret an array of pixel map into a digit
Print Screen	Print the screen and get a image
Row to Column	Transform a 2D array of a single column into a 1D array
Temperature PID Action Engine	Start, control and close the PID temperature control
Temperature PID	A stand alone temperature PID control VI
Timer	Provide the same elapsed time line for different loops
Vpower Action Engine	Start, read from, write to and close the power supply

3.2.1 FTIR Control and Data Transfer

The FTIR (Spectrum Two) is directly controlled by the official software called Spectrum 10 (hereinafter referred to as Spectrum Two Software or ST software). It is possible to communicate with Spectrum Two via USB. But since all what is needed of this instrument to do is simple, it is not necessary to study the USB communication protocols of Spectrum Two which is very complicated.

To control the Spectrum Two a FTIR Server VI was created. In the set up of the ST software, make it export an .CVS file of the spectrum in a certain folder every time the acquirement of a spectrum is finished. The FTIR Server will keep checking the file status of the same folder continuously. When a new file is detected the program will send this file to the Main Control VI through Ethernet. When the Main Control VI receives a spectrum it knows that a full scan has finished and will send a message “CLK” to the FTIR Server to ask for a “click”. Then the FTIR Server will move the cursor over the SCAN button of the ST software and do a click to get another scanning started. During this cooperation between FTIR Server VI and ST software, no application interface is used.

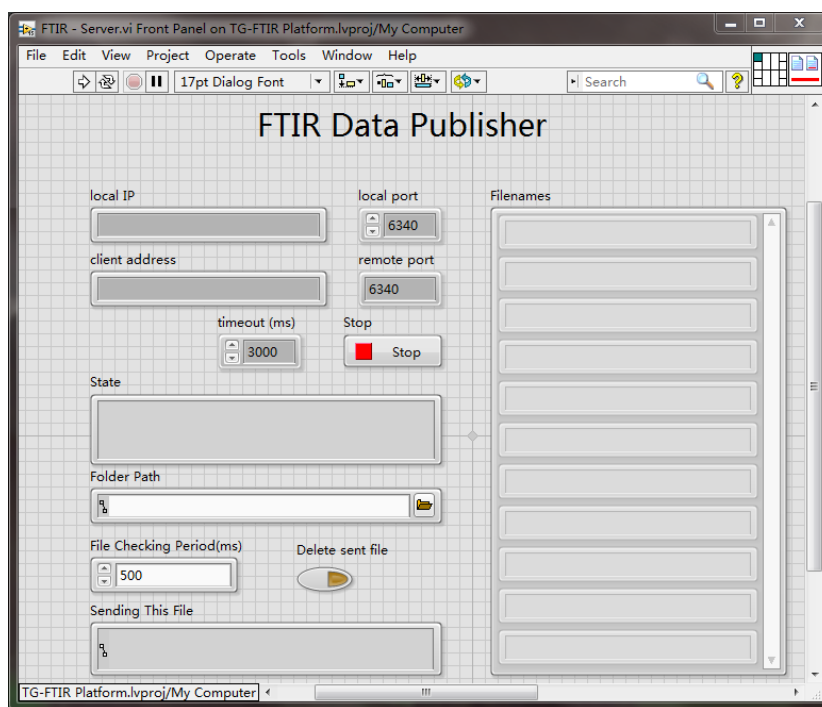


Figure 36. FTIR Server front panel.

The FTIR Server is a stand alone VI and was packaged into a installer and distributed on the computer where ST software is. After installation the first thing to do is to input the folder path of the CVS file and set the communication port, then it is ready to run as a server. In the Local IP text box the local IP is displayed for the use to fill in the Main Control to establish a connection.

The FTIR Server VI has a Detecting New File Loop(Fig. 37) which keeps running none stop. At the beginning of every loop, it get a list of all the files in the designated folder. The new list acquired in the next run is compared with the old list. For every element in the new list, if it does not exist in the old list the case structure will execute

the 0 case in which the file will be put into a queue as a 2D array. The TCP Server Loop will send this 2D array to the Main Control.

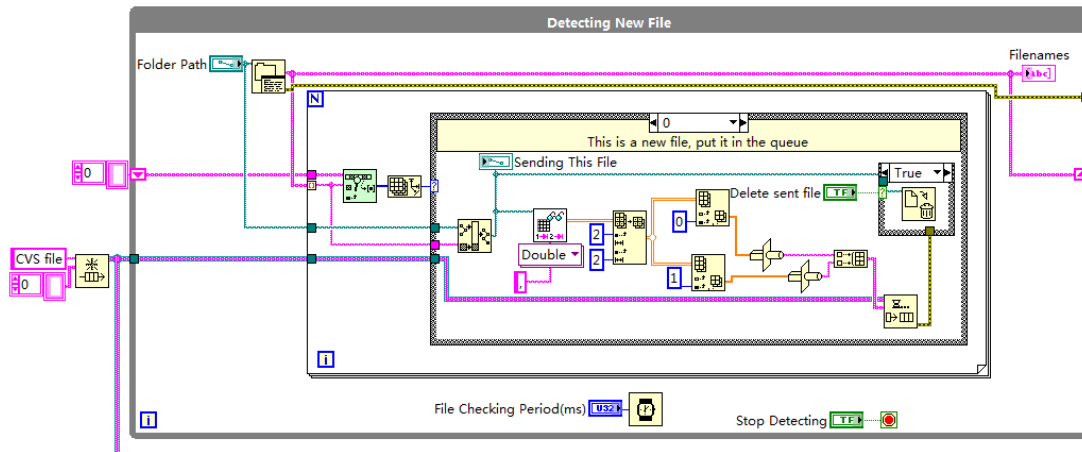


Figure 37. Detecting New File loop of FTIR Server

The TCP Server Loop (Fig. 38) is the most important part of the FTIR Server VI. Since this app is designed as a server it needs to run continuously without the need for operation. The design pattern of this loop is a state machine. It has four states: listen, send, handle error and close. It works only in one state but will keep transfer into other states as needed. Normally it is in listen state in which it will wait at the specified port for TCP connection. If no connection is established, it waits for a certain amount of time (here set as 1 second) and goes into handle error state which will come back to listen state later after error handling. Simply put, this loop will keep listening while making sure there is no errors that could potentially prevent a connection. If a connection is established it goes into the send state and stays in there as long as the connection is not aborted. In the send state the loop will check the CVS queue. If the Detecting New File Loop has placed some data in the queue, the data will be put in the Ethernet stream to the

Main Control. If no data is in queue for sending, it will send a message of “Stand by” to the Main Control. The send state is also able to read the message from the Main Control. So far there are two messages designed: CLI-click, CLO-close. “Click” means the Main Control is requiring another scan. The click on the Scan button of ST software is performed by the code in Fig. 39. “Close” command will cause the send state to terminate and transferred to handle error state, in other words, into idle state.

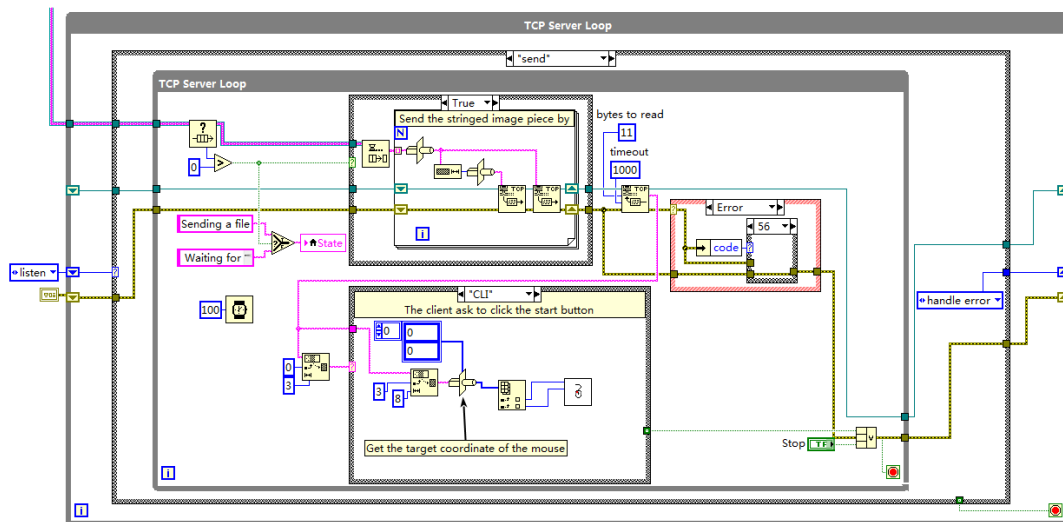


Figure 38. TCP Server Loop

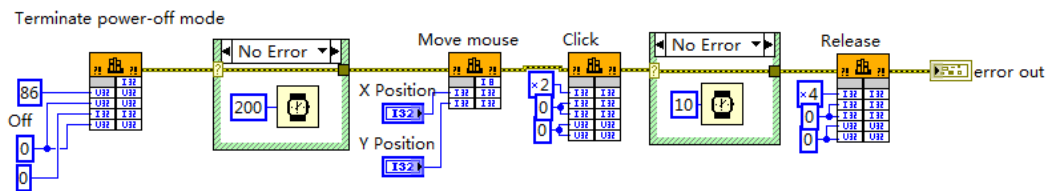


Figure 39. Mouse Click Event triggering

3.2.2 TGA Server

A mechanical micro-balance requires sophisticated feedback control. The direct control of the balance refitted to this system is difficult and is not necessary if there is easier way. The TGA 2950 has a full control circuit and well programmed embedded system. GPIB protocol is used to communicate with TGA 2950. Some efforts was put into using GPIB to communicate with TGA 2950 but was not successful. One more step back, the TA Instrument Control software (hereinafter referred to as TA software) is able to communicate with the TGA 2950 with a GPIB cable and the mass data is updated on its user interface. But there is no application interface for third-party developers. A bold solution was proposed to use image recognition to acquire the mass data from the screen. Image processing is an advanced programming technique and usually requires high level mathematical algorithm. But this method was achieved at last and the mass data was successfully collected.

The TGA Server VI is created to capture the screen of the TA software and send it to the Main Control PC. The image recognition is performed by the Main Control VI. Same as the FTIR Server VI, the TGA Server is also a stand alone VI built into an application package and distributed on the PC where the TA software is.

Fig. 40 is the user interface of the TGA Server. Local port also need to be specified for TCP/IP communication. An image path is specified for the image acquired to be stored before it is transmitted.

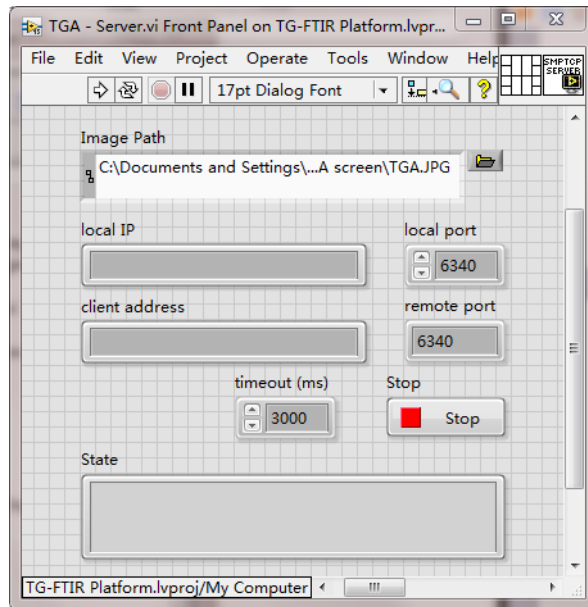


Figure 40. TGA Server front panel

The TGA Server (Fig. 41) has one loop which is a state machine. It has three states: listen, send, close and handle error. The close state is not usually used because this application is supposed to be data server and can be connected anytime from the Main Control VI. Very similar as that of the FTIR Server, this state machine keeps listening and enter handling error when no connection attempt is detected. When a connection is established it will enter the send state. Two sub VIs are used here: Print Screen and Image to String (Fig. 42). The Print Screen VI captures the whole screen and store the image in a designated folder. The Image to String VI read the image file and convert it into a formatted string. The image can be restored according to the format from the string.

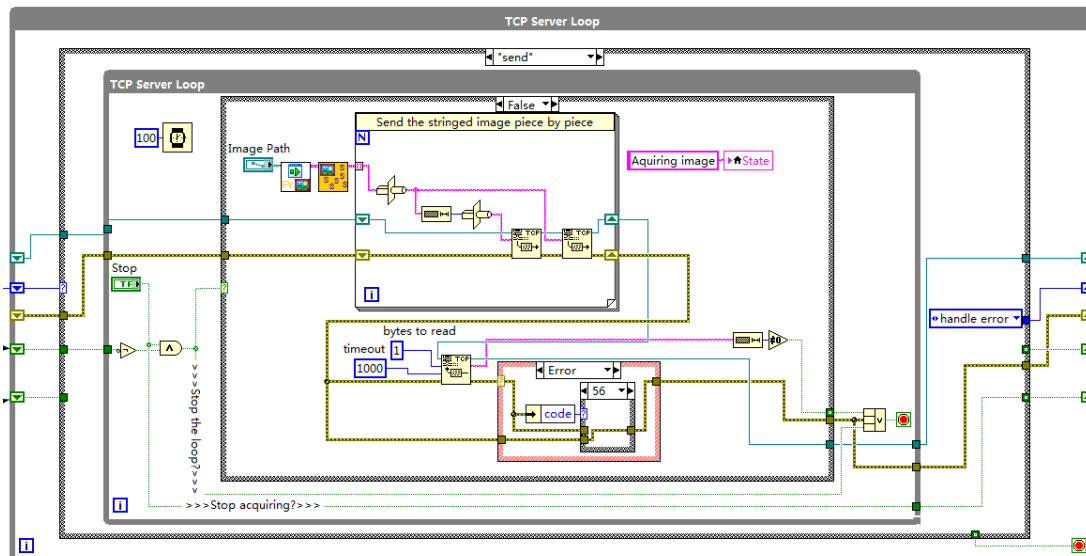


Figure 41. TGA Server block diagram

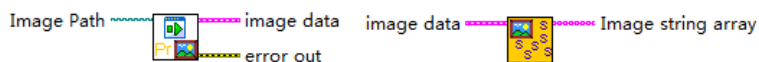


Figure 42. Print Screen VI (left) and Image to Data V I(right)

3.2.3 Main Control

The Main Control was distributed on the operation computer. It has three major functions: receive and process the TGA data, control the FTIR and receive its data, control the furnace temperature.

This Main Control VI (Fig. 42) is the only application that the user need to interact with. When all other devices are well configured, the user will be able to start an experiment by running this software. Fig. 42 shows the user interface of the Main Control VI. For the first run of this application, the FTIR server and TGA server IPs and ports need to be filled in. The top graph shows the most recent IR spectrum received. The smaller graph shows the mass and temperature history. The server message shows

status of the FTIR Server. Every time a spectrum is received a “Stand by” should show up indicating that the FTIR is in idle. The target temperature and heating rate is specified in another user interface.

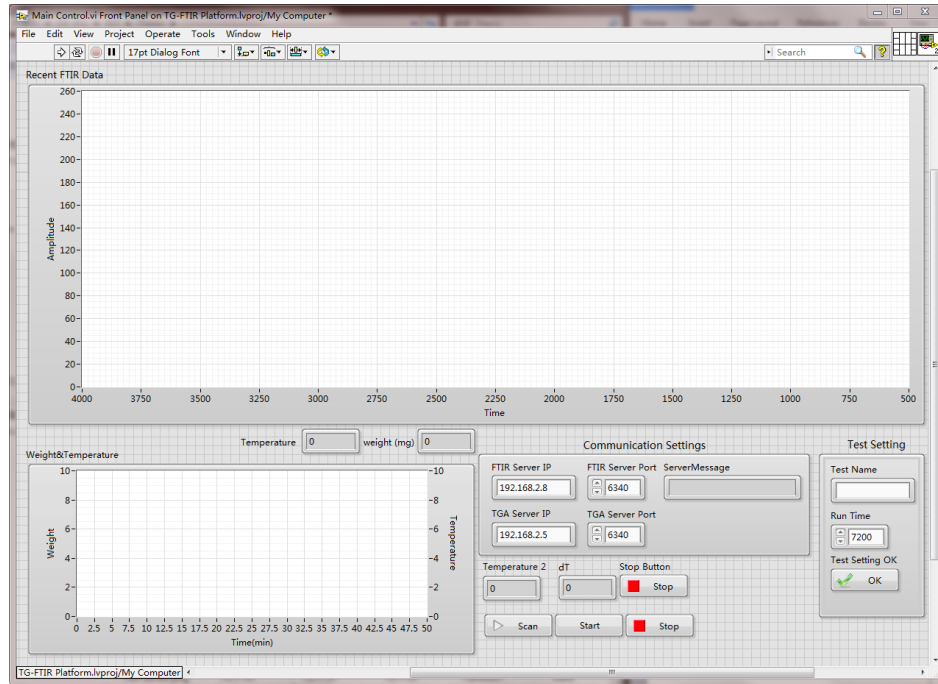


Figure 43. Main Control VI user interface

There are totally four loops in the Main Control: TCP Client for TGA, TCP Client for FTIR, Event Handler and Temperature Control. Each loop can operate independently.

Fig. 43 shows the TCP Client Loop for TGA. Since the TGA Server sends the images in formatted strings. The images first need to be restored from the strings before it can be recognized. A complete image has four major parts: 1. the dimension, 2. the image itself(pixel array), 3. mask, 4.the colors. The four parts are all sent in arrays. Each part is read and filled into an image template. When all four parts are filled, an image is complete and ready to be shown. The image is interpreted into a number by Image to

Number VI (Fig. 44). This VI has a for loop which will run 7 times. The original image is a whole computer screen which is too big for analysis. A subset of the image pixel array is taken to locate at where the mass data is to get the “number image”. The “number image” is breaking down further into seven and becomes “digit images”. The seven “digit images” contains the six digits of the mass data number and one decimal point. The 7 runs will interpret the 7 “digit images”. Number Recognizer VI (Fig. 45) is created to get the digit from the digit image element.

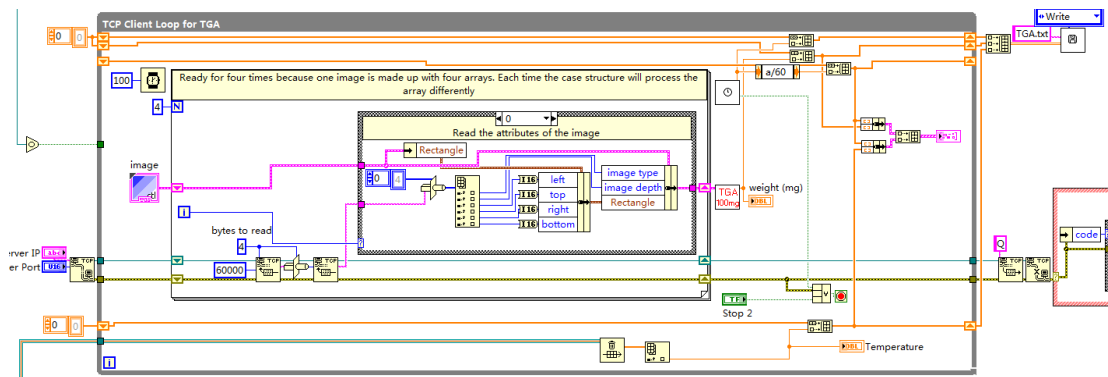


Figure 44. TCP Client Loop for TGA

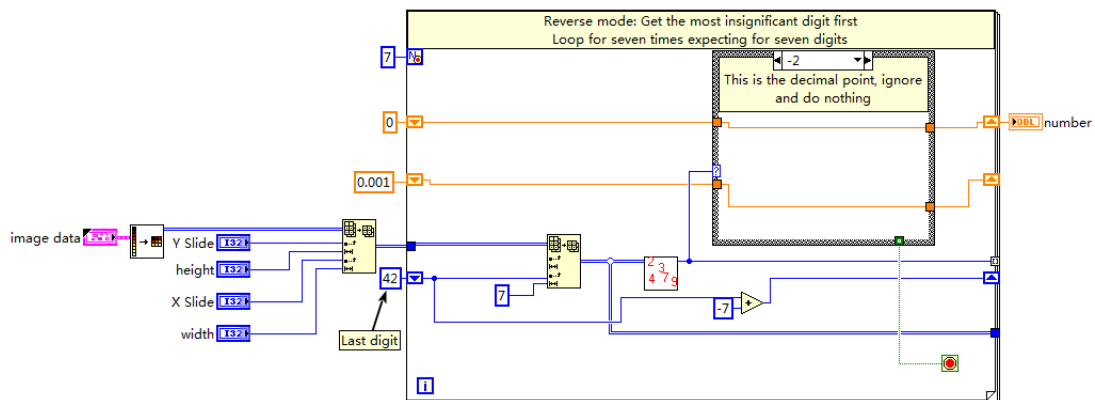


Figure 45. Image to Number VI block diagram

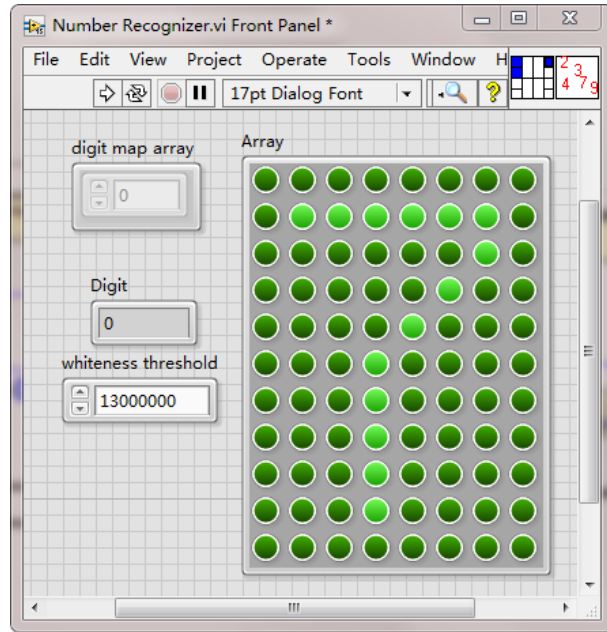


Figure 46. Number Recognizer front panel. A seven is displayed in a Boolean array indicator

The Number Recognizer first convert the digit image into a simple array of 0 and 1 by comparing the pixel array element with a whiteness threshold. If the number for the pixel is less than the threshold, it is considered 0, otherwise 1. By summing the array up we get the primary identification of the digit by referring to Table 9.

Table 9. Digit test

Sum	Digit
4	Decimal point

5	Minus sign
13	1 or 7
15	3
16	2 or 5
18	0, 6 or 9
19	8
20	4

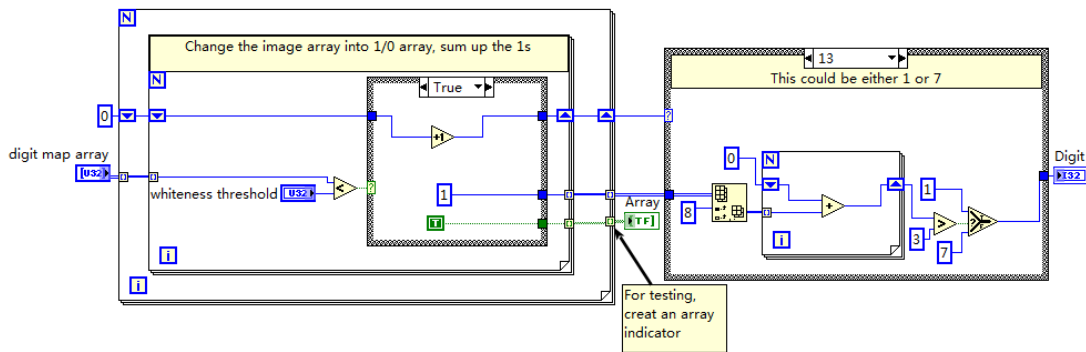


Figure 47. Number Recognizer VI block diagram

To differentiate digits which have the same number of dark pixels some further comparison is needed. For example, 1 and 7 have the same number of dark pixels, but one can compare the dark pixels on the 9th row where the bottom of 1 has 4 pixels while 7 has only one. With similar technique one can figure out 2, 5, 0, 6, and 9.

The program starts from the least digit and multiply it by 0.0001. The next will be multiplied by 0.001 etc. The decimal digit image is actually be ignored. By summing all

the component number up the mass number can be obtained. It is not common but if an minus sign appears this number will be multiplied by -1.

Fig. 47 shows the TCP Client Loop for FTIR. The IR data are sent in the form of arrays and are written to the disk with the File Action VI. The Timer VI provides the experiment time to be used at a part of the file name.

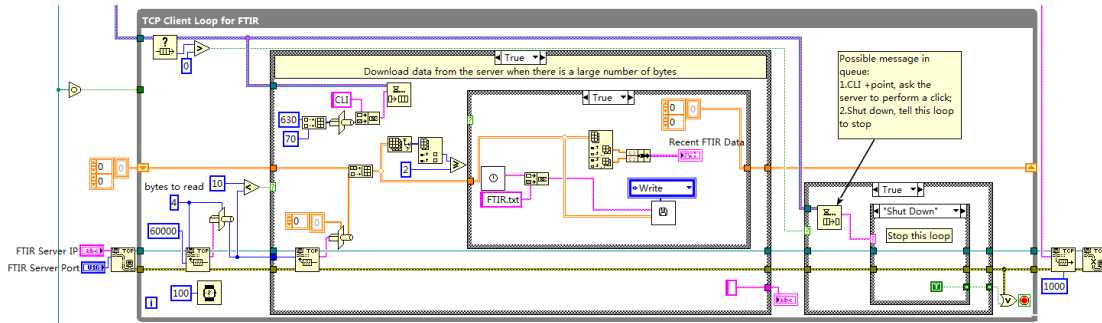


Figure 48. TCP Client Loop for FTIR

The temperature control is achieved by the Temperature PID Action Engine VI. This VI is further addressed in the next chapter.

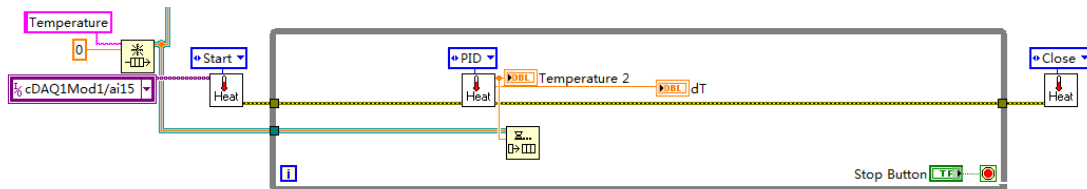


Figure 49. Temperature Control Loop

3.2.4 Temperature Control

The Temperature control is achieved by the Temperature PID Action Engine VI. This VI is not an independent application as the TGA Server or Main Control, but due to its complexity and potential to run independently it is addressed in separate chapter.

For thermal analysis temperature control is very important. With PID (proportional, integral, derivative) control algorithm, it is very easy to set the furnace temperature at a fixed point. There are many commercial PID temperature controllers available. These controllers usually measure the temperature of a thermocouple and use a relay to turn the heating component on and off. These controller works very well for setting a system with relatively big heat capacitance at a temperature set point and keep it stable when some external disturbance occurs. If the thermal system is small and has little heat capacitance, the heating and cooling will both be rapid. Most commercial temperature controllers for lab use can not react fast enough. Even though the controller can mathematically provide, the working principle of change working load portion of a cycle can not provide a fine control. On the other hand, it is not possible to perform a temperature ramp with a normal commercial temperature controller.

In the TG-FTIR instrument, restricted by the DRIFT chamber, a very small furnace has to be used. To guarantee the high temperature the power of the furnace can be very high(over 100W). This is a typical small capacitance system. For experiment need, temperature ramp at different rate is a necessary.

The temperature control system includes the furnace, programmable power supply and the Temperature PID Action Engine VI. The programmable power supply allows

dynamic setting of voltage and current(only one parameter can be set at one time) with a readability of 0.01. It provides finer control of the heating power. This power supply is the base of adopting more dedicated programming control.

Fig. 49 shows the front panel of the Temperature PID Action Engine VI. As mentioned before the Main Control VI does not have settings for crucial experiment parameters of the target temperature and heating rate. It is because there are many other settings used in temperature control like the PID gain, the initial current, the voltage set point also need to be changed sometimes. But for the purpose of focusing on the experiment those programming work are avoided. The initial current for the power supply varies a lot for different temperature ramps and for the most common ramps, the suggested values are listed on the front panel.

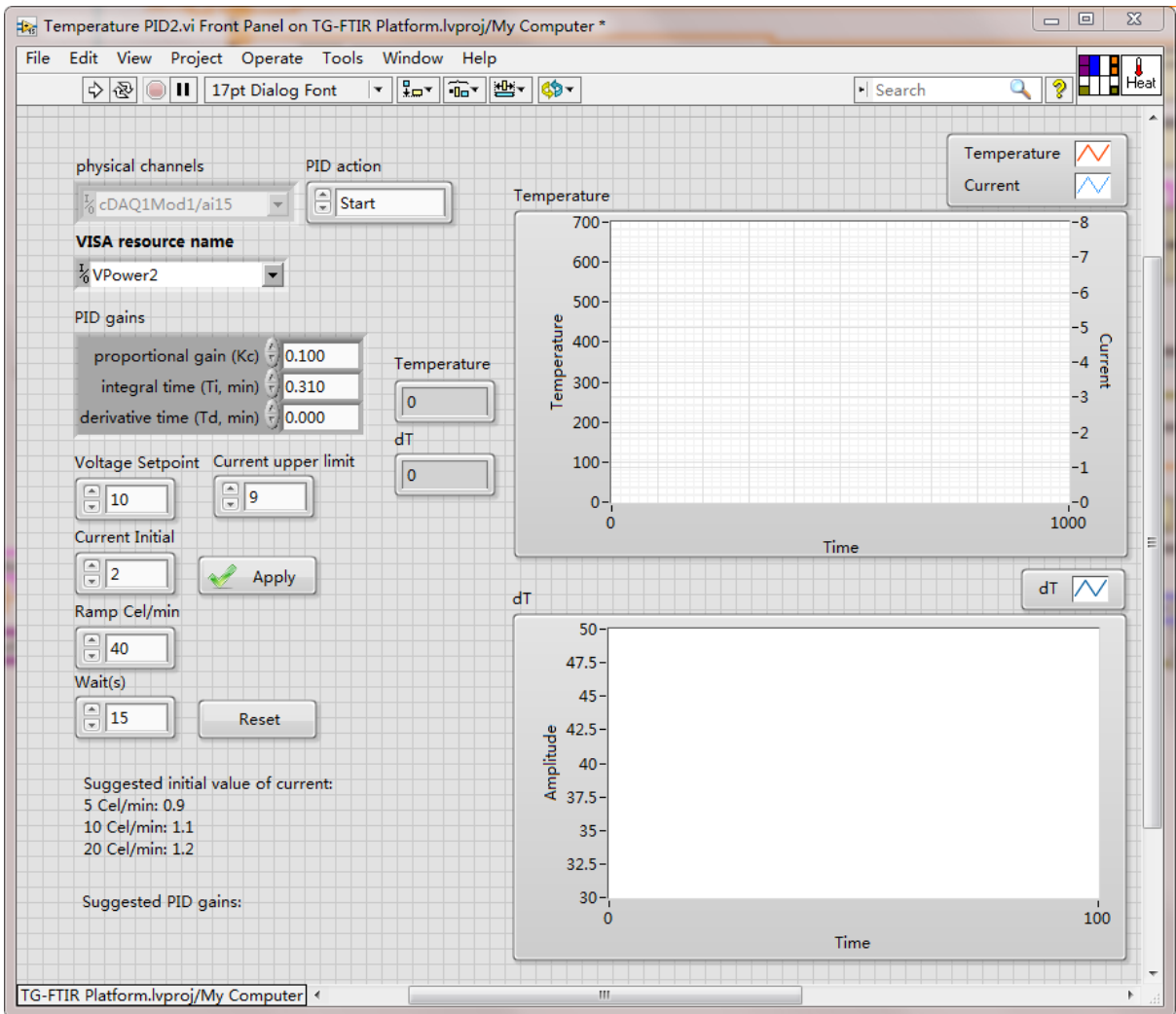


Figure 50. Temperature PID Action Engine VI front panel

Fig. 50 shows the loop of the Temperature PID Action Engine VI. The Analog Input Action Engine VI is used to establish a channel to read the temperature of the thermocouple. The VPower Action Engine VI is used to read the current and set the current of the power supply. These two VIs are gate of the virtual code to the physical world.

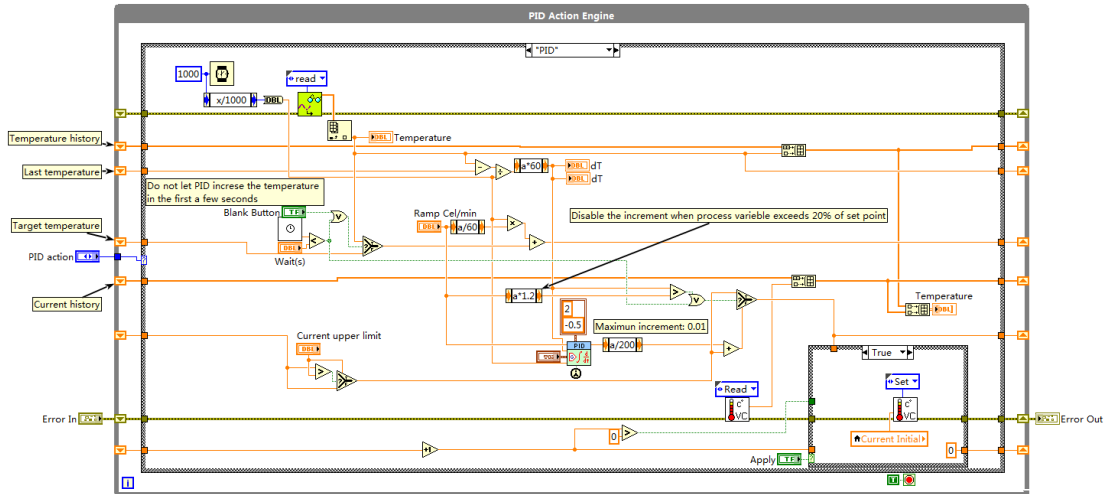


Figure 51. Temperature PID Action Engine VI block diagram

The core of this code is still the PID algorithm. Table 10 shows the main parameters of the PID module:

Table 10. PID gains

PID gains	Values
Proportional gain (K_c)	0.1
Integral time (T_i , min)	0.31
Derivative time (T_d , min)	0.00

For this PID module the control variable is the current increment and the process variable is temperature rising rate. The range of the control variable is set to be within $-0.0025 \sim 0.01A$. For an object with no heat loss, the temperature should rise in a constant rate if heated with constant power assuming the heat capacity is a constant. This still applies to objects with good insulation at relatively lower temperature. So the power needs to increase only a little bit to make up for the heat loss to the environment. Thus the basic concept for heating the furnace is to hold to the heating power and increase the

power little by little. This is why the range for the control variable is set to be very small and has little in the negative range(dropping the heating power is almost unnecessary). The better insulation the furnace has, the smaller range the temperature increment range should be.

A further approach to ensure the steadiness of the temperature increasing rate is to set a limit on the execution of the PID module. Here if the temperature increasing rate is already higher than 20% of the set point, the PID output will be disabled and will not be able to increase the current.

Fig. 51, Fig. 52 and Fig. 53 showed the temperature control testing result each heating at 5 °C, 10 °C and 20 °C. The temperature curves are very straight indicating a constant rising rate as set.

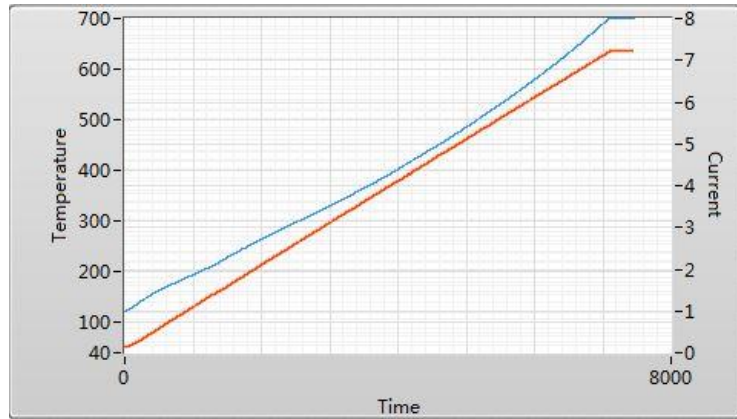


Figure 52. Temperature control test, 5 °C/min

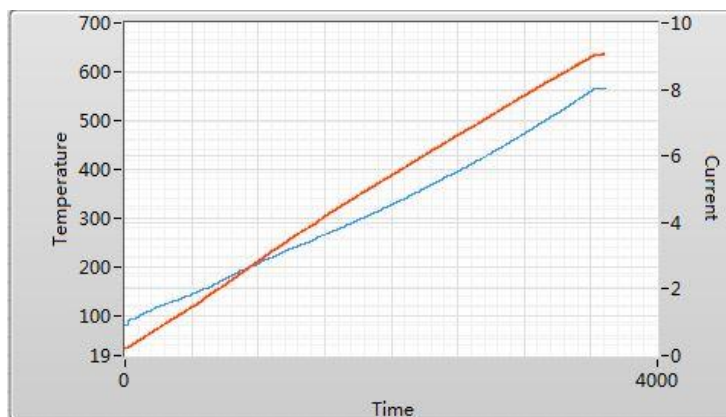


Figure 53. Temperature control test, 10 °C/min

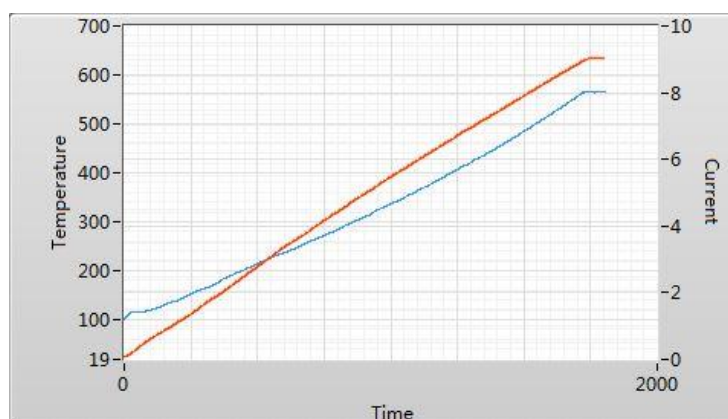


Figure 54. Temperature control test, 20 °C/min

3.3 Experimental test

Calcium oxalate monohydrate ($\text{CaC}_2\text{O}_4 \cdot \text{H}_2\text{O}$) is also known as whewellite is chosen to test the TG-FTIR instrument. Calcium oxalate monohydrate is a standard sample for TGA because it has three significant weight loss stage and the last one appears at relatively high temperatures (over 700°C). Meanwhile the oxalate and hydroxyl it

contains many characteristic IR absorption lines. Besides during its decomposition process the sample does not have a significant geometry change. This provides a good IR wave path. With all these reasons calcium oxalate is made one of the best testing sample for this instrument.

The very first step of $\text{CaC}_2\text{O}_4 \cdot \text{H}_2\text{O}$ decomposition when heated involves the loss of water and the formation of anhydrous calcium oxalate. In the second step calcium oxalate lose carbon monoxide and decompose into calcium carbonate. In the final step the calcium carbonate lose carbon dioxide and decompose into calcium oxide.

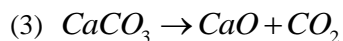
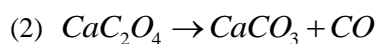
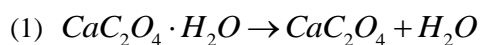


Table 11. $\text{CaC}_2\text{O}_4 \cdot \text{H}_2\text{O}$ theoretical wight loss

Step	Theoretical stoichiometric weight loss(%)
1	12.3
2	19.2
3	30.1

3.3.1 Experiment

CaC₂O₄·H₂O (99%) was obtained from Alpha Aesar. 11.939 mg CaC₂O₄·H₂O was loaded onto a platinum pan. The IR background scan was taken on the sample at its original status. The FTIR was set to scan from 4000 cm⁻¹ to 500 cm⁻¹, resolution of 4 cm⁻¹, accumulation of two scans. The heating rate of the furnace was approximately 14 °C/min. It is worth noticing that when this experiment is carried out the Temperature PID Action Engine VI has not yet been developed. During the experiment the temperature was manually controlled by turning the power supply current knob.

3.3.2 Results and discussion

The TGA thermogram for the CaC₂O₄·H₂O is shown in Fig. 54. Three weight loss steps are clearly illustrated. For the first two steps the data matches the theoretical data very well. The final step of the decomposition of calcium carbonate did not finish due to the failure of further heating of the furnace.

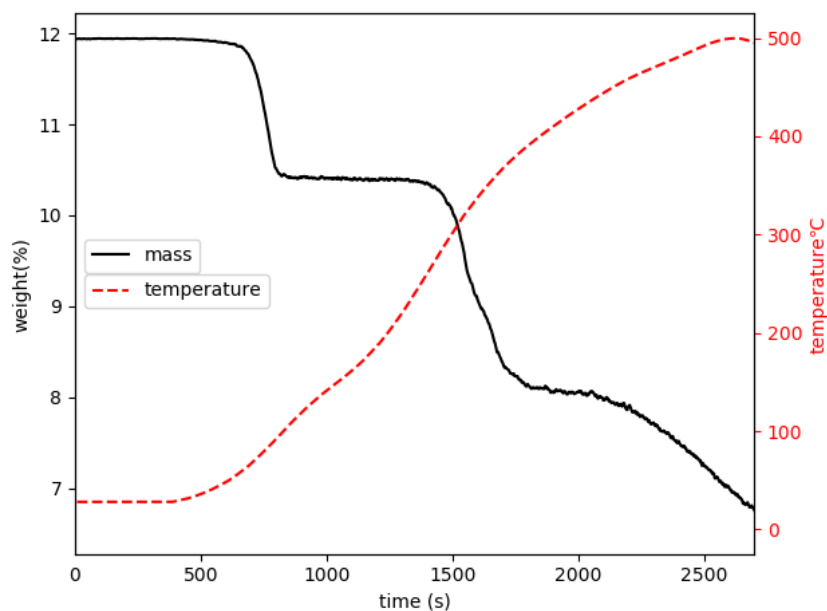


Figure 55. Thermogram of Calcium oxalate decomposition

Table 12. Experimental weight loss

Step	Theoretical stoichiometric weight loss(%)	Measured weight loss%
1	12.3	12.9
2	19.2	19.56
3	30.1	?

The third step was suppose to happen until 600°C but in this thermograph it started at 480°C. This could be caused by the uneven heat transfer and inaccurate temperature measurement. In this experiment the sample pan is hooked by a metal wire from the top for mass measurement, thus can not be touched. The thermocouple has to be placed at the side of the sample pan with no direct contact. Unlike in a sealed tube furnace where the temperature around the center is relatively even, the specially designed furnace for

this experiment can only heat the sample pan from below. This arrangement end up with significant temperature gradient across the small sample pan. The sample at the top surface of the sample could be of more than 100°C lower than that at the pan bottom where it has direct contact with the hot pan. This could lead to the result that the sample at the bottom has already started the decomposition of the third step but the sample at the surface is still waiting for higher temperature.

Fig. 55 Shows the standard IR spectrum of calcium oxalate monohydrate. There are many vibration bands. The most significant ones are chosen to be studied with our instrument.

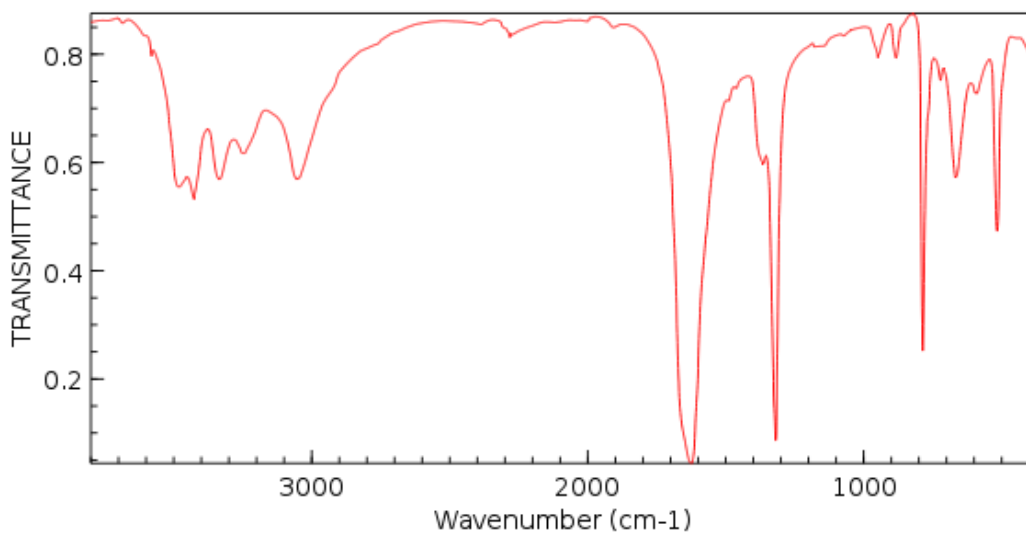


Figure 56. Standard Calcium oxalate IR spectrum(NIST Chemistry WebBook)

Table 13. Calcium absorption lines and assignment

Wavenumber cm^{-1}	assignments
3495	$\nu(\text{OH})$
3440	$\nu(\text{OH})$
3340	$\nu(\text{OH})$
3250	$2\delta(\text{HOH})$
3060	$\nu(\text{OH})$
1645	$\delta(\text{HOH})$
1620	$\nu_9(\text{ox}): \nu_a(\text{CO}_2)$
1483	$\nu_1(\text{ox})(?): \nu_s(\text{CO}_2)$ and $\delta(\text{HOD})$
1460	$\nu_1(\text{ox})(?): \nu_s(\text{CO}_2)$ and $\delta(\text{HOD})$
1380	$\nu_1(\text{ox})(?): \nu_s(\text{CO}_2)$
1365	$\nu_{11}(\text{ox})(?): \nu_s(\text{CO}_2)$
1386	$\nu_{11}(\text{ox})(?): \nu_s(\text{CO}_2)$
943	$\nu_{B'}(\text{H}_2\text{O})$
880	$\nu_{B'}(\text{H}_2\text{O})$
782	$\nu_{12}(\text{ox})(?): \nu_s(\text{OCO})$
765	$\nu_{12}(\text{ox})(?): \nu_s(\text{OCO})$
656	$\nu_{B''}(\text{H}_2\text{O})$
625	$\nu_3(\text{ox}): \omega(\text{CO}_2)$
600	$\nu_{B''}(\text{H}_2\text{O})$
513	$\nu_7(\text{ox}): \omega(\text{CO}_2)$

In IR spectroscopy absorption can be used to for quantification study according to Beer's law:

$$A = -\log T = \log \frac{P_0}{P} = \epsilon bc \quad (11)$$

Where T is the transmittance, P₀ is the light intensity through the sample, P is the light intensity of blank, ε is the molar absorptivity, b is the path length and c is the concentration.

Absorbance is in linear positive correlation with the concentration while transmittance is in negative logarithmic correlation with the concentration. In this experiment the IR spectra are in transmittance. Besides IR background was taken on the sample itself thus the transmittance can not be converted into absorbance. But still the concentration is in a negative correlation with the transmittance. Namely, the lower the transmittance, the higher the concentration.

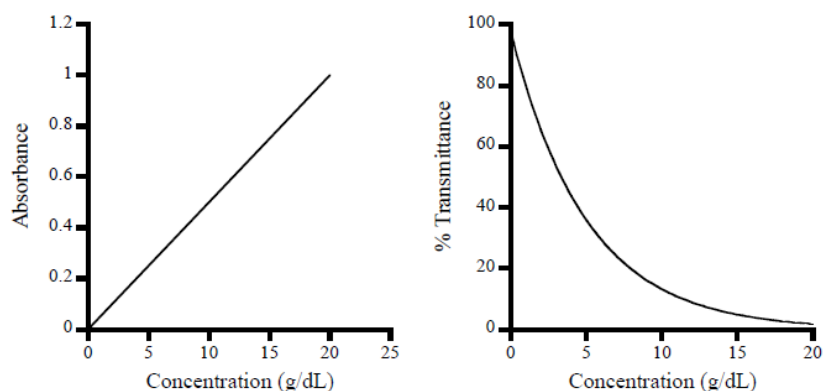


Figure 57. Correlation of the absorbance and transmittance with the concentration

Fig. 57 is a full collection of all IR spectra during the experiment. The Z axis is the transmittance and the bottom plane is wavenumber and time. By cutting along the axis of wavenumber, one can get the cutting edge of a normal transmittance-wavenumber curve like a common FTIR spectrum. The data beyond 700 cm^{-1} is ignored because of high

noise. By cutting along the axis of time one can get the cutting edge of transmittance-time (hereinafter called TT curve). One can cut at any wavenumber and get the trend of transmittance of that wavenumber all over this experiment.

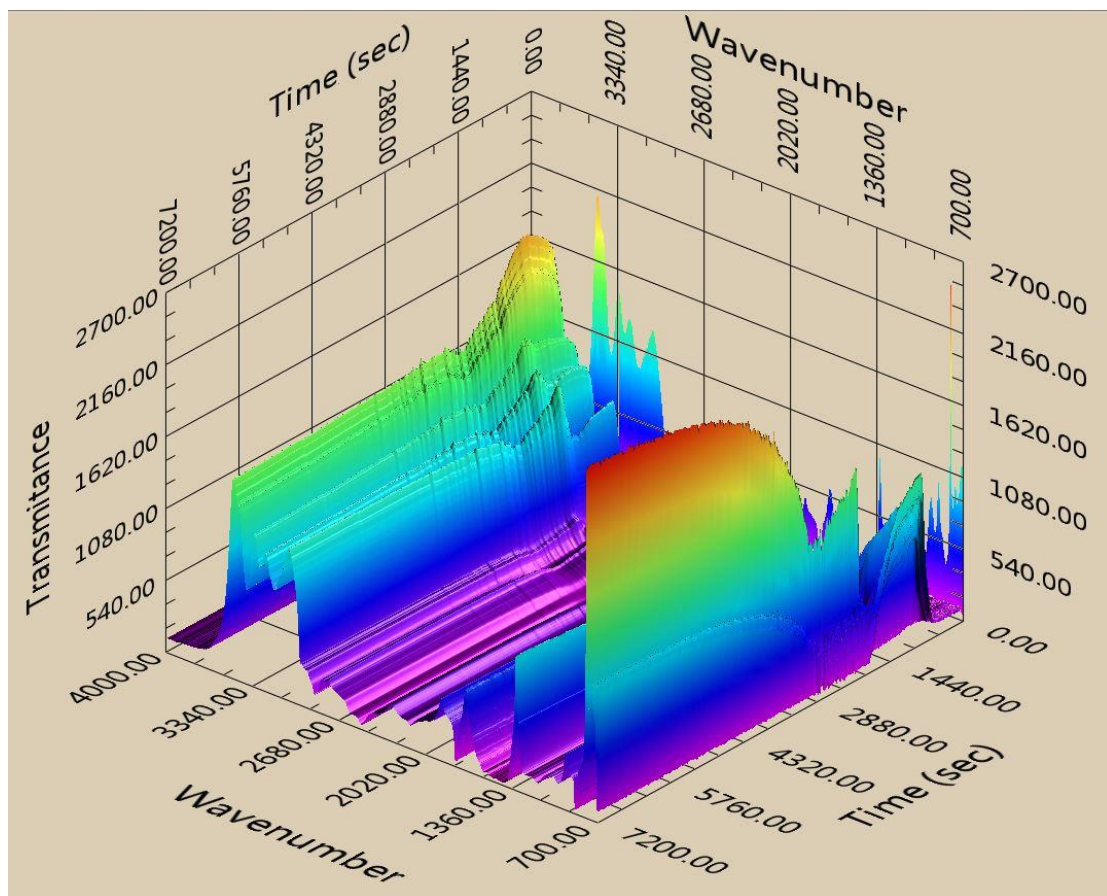
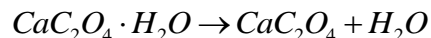


Figure 58. All IR spectra in 3D

Fig. 58 shows the TT curve of a OH vibration band at 3492cm^{-1} . Since transmittance is in negative correlation with the concentration, it is obvious that there is a big loss of the OH group during the first stage of the heating process. By combining the TG curve and the TT curve one can perform some further analysis. There are mainly four segments in this TT curve. The first one is flat like the TG and temperature curve as the heating

process has not yet started. The second segment is a sharp rise. Its beginning and ending both matches the first step of the TG curve as the following reaction is going on:



This also proves that the observed OH group belongs to the water molecules. In the flat region of the TG curve between the two steps, the TT curve still shows a gentle slope until the second significant drop of the TG curve begin. It is well known that the second decomposition has not yet started and calcium oxalate monohydrate is a simple compound, the rise of the TT curve should still indicate the loss of water molecules. There are potentially two reasons. First, some crystalline water molecules had stronger combination in this compound. Second, it is could be that there was only one type of combination but due to the uneven temperature distribution in the sample pan, the water molecules was not completely released in the first step and the loss of water molecules continued until the second step.

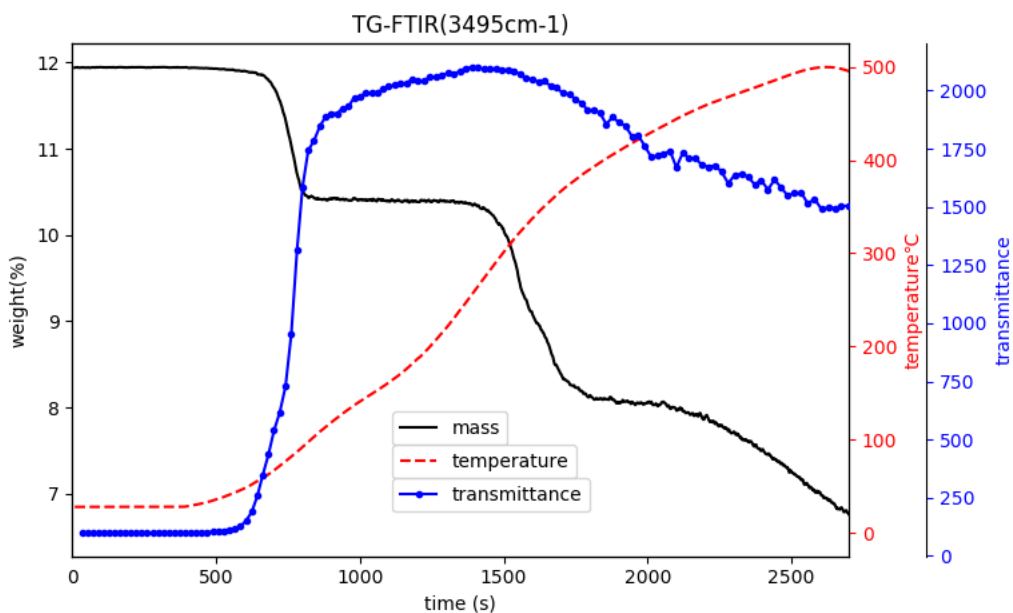
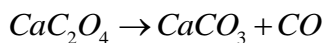


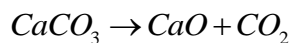
Figure 59. Comparison plot at wavenumber 3945cm^{-1}

The fourth segment of the TT curve is a gradual drop. This seems to indicate a formation of OH bonds but the experiment condition of continuous heating will not allow that. In the second step calcium carbonate is formed which also has absorption at 3495cm^{-1} thus bring the transmittance back down.



All other four absorption lines of OH between 3500 cm^{-1} and 3000 cm^{-1} has similar TT curve like the one in 3495 cm^{-1} .

The absorption line in 880 cm^{-1} is assigned to H_2O vibration but its TT curve (Fig. 59) shows very different trend. Like in the TT curve at 3495 cm^{-1} , in the fast rising segment indicated the loss of water molecules reasonably. The segment at the flat region of the TG curve between two steps is a gradual drop and is hard to explain because there is supposed to be no reaction going on in this period. The segment during the second step of the TG curve is a steep drop to the bottom. In the second step the following reaction is on:



The calcium oxide IR spectrum shows that the calcium oxide has strong a strong absorption line near 880 cm^{-1} which should be the reason of the drop in the second decomposition step.

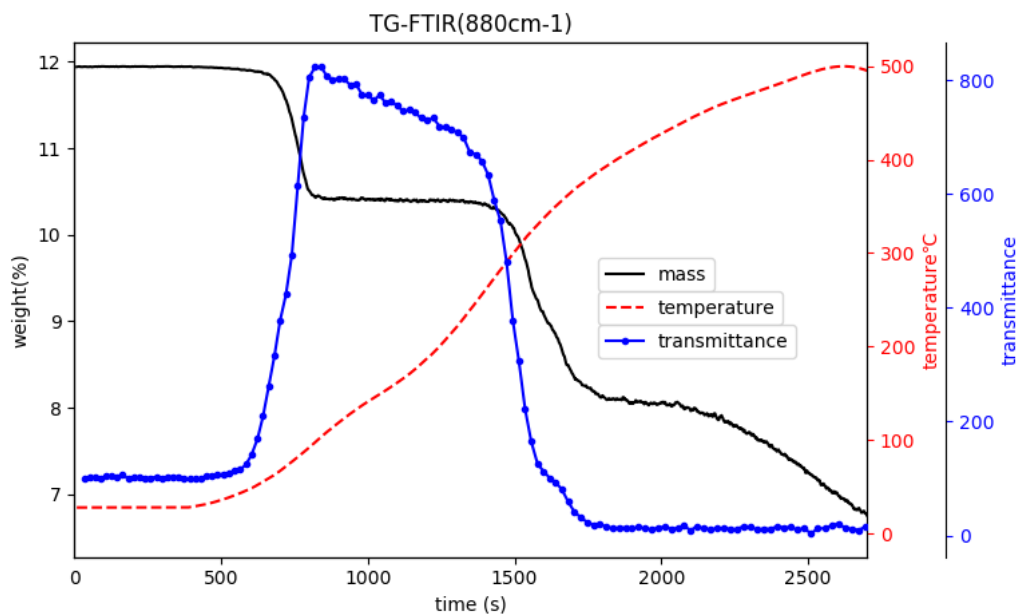


Figure 60. Comparison plot at wavenumber 880 cm^{-1}

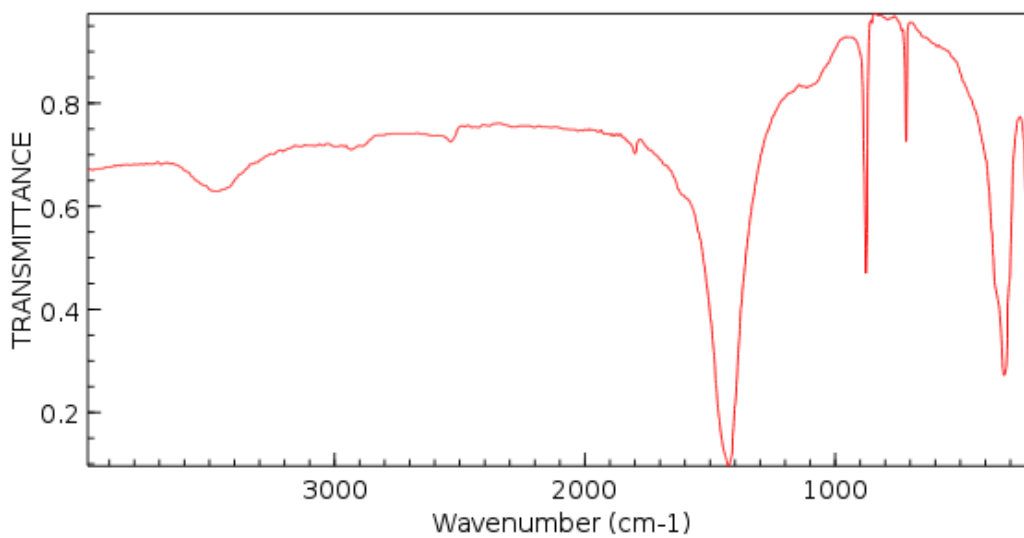


Figure 61. Standard IR spectrum of calcium carbonate(NIST Chemistry WebBook)

The absorption line at 782 cm^{-1} is assigned to stretching oxalate and in plane bending of OCO group. The TT curve is shown in Fig. 61. This TT curve stays flat and begins to

have a rapid rise right at the end of the second step of the decomposition indicating loss of oxalate. By the TG curve, the loss of oxalate started at about 1450s, but the TT curve only indicate the loss at around 1700s when the all the calcium oxalate has being converted into calcium carbonate. This coincided with the assumption that the temperature distribution in the sample is very uneven. Because the in-situ FTIR only monitors the surface of the sample where the temperature was the slowest to rise. The change only occur at TT curve when the sample at the top undergo the reaction.

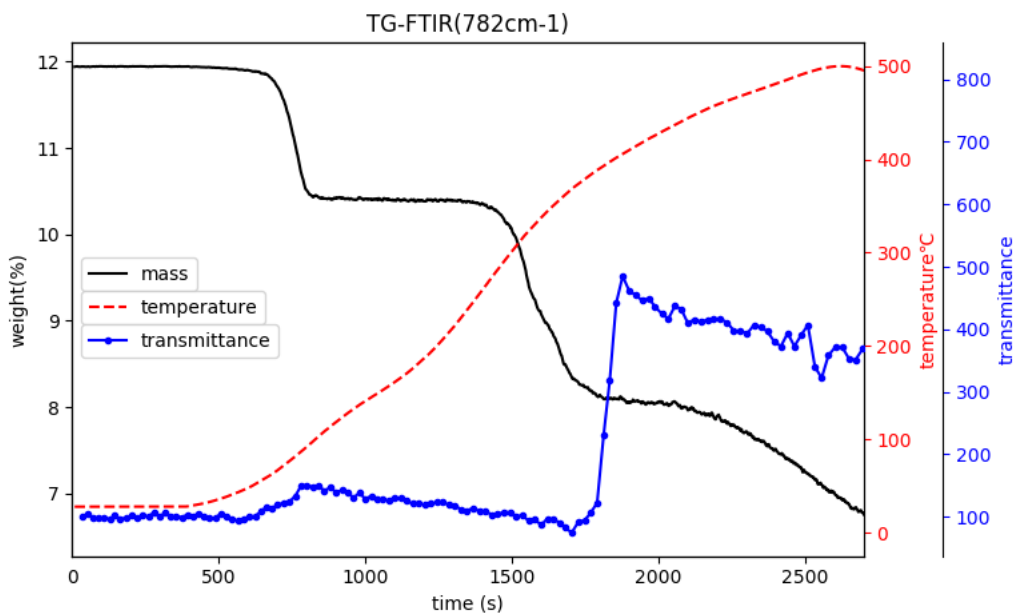


Figure 62. Comparison plot at wavenumber 782cm^{-1}

3.3.3 Conclusion

There are thousands of TT curves you can look into in this whole data set. The TG curve and the TT curve acted as mutual evidence. Some changes in TG curve is not observed but showed great change in the TT curve. The opposite is also true.

By conducting the calcium oxalate decomposition experiment, the instrument accuracy and reliability is tested. The thermogram of calcium oxalate decomposition matches very well with the theoretical result. That means the accuracy is not lost when refitting the micro balance and the software implanted to work with the TA software acquired and transferred the mass data with no mistakes.

The temperature control was not very satisfying and the temperature was not high enough to finish the third step of the decomposition. The temperature control unit consisting of the software described in 3.2.4, the programmable power supply and the newly built furnace has been developed after this testing experiment. As the temperature test result shows, the temperature control can be good enough now.

The IR spectra were successfully acquired in-situ. The transmittance of a certain wavenumber was plotted together with the weight along the time axis. The analysis showed that the two data are mutual evident in revealing the mechanism of the decomposition process. This is the advantage of instrument integration. One change in the thermogram may show different changes by looking at different wavenumbers in the IR data. The comparison analysis of TT curves at 880cm^{-1} and 3945cm^{-1} has proved this very well.

The experiment shows that this TG-FTIR system functions as designed. There is no problem is data acquisition transfer and storage. The measurement accuracy and repeatability is pretty good. The different data it acquired in parallel were in reasonable correlation with each other.

4 SUMMARY AND PROSPECT

This research served for the purpose of developing in-situ characterization instrument for material chemistry. Among many characterization methods IR spectroscopy was chosen for simple operation condition being safe and its capability to reveal rich structural information of materials. To break critical barriers of the instrumentation integration, two projects have been carried out to study IR instrumentation and integrating IR spectroscopy with TG.

In the first project the working principle of FTIR was fully studied and explored. The mathematics and computation method of Fourier transform was demonstrated. By simulating the signal produced by the optical system of the instrument, the signal acquisition and processing methods were developed and tested. The hardware were set up and software developed. The alignment of the Michelson interferometer with IR was not successful due to the complexity brought by the invisibility of IR. But experiments using white light succeeded and interference patterns were observed. Once the alignment is achieved with proper skill, FTIR technique can be modified, simplified and diversified. More effort can be poured on time resolved spectroscopy etc.

The second project was a straightforward setup integrating FTIR and TGA, during which there were many challenges because the similar setup has never been done before. The hardware and software development were both successful and the experimental tests showed good accuracy, reliability and repeatability. The experiment results also demonstrated the uniqueness and value of the data. With this instrument, most thermal analysis can be equipped with IR spectra. Different from commercially available TGA-FTIR combined system in which the FTIR only perform analysis on the evolving gas, this instrument provides IR spectra of the sample itself. With enough funding and investment, it is easy to lift the quality of this instrument. With better precision balance more accurate mass data can be acquired. With a well designed DRIFT optical chamber, reaction atmosphere can be controlled. By studying the temperature interference on IR spectrum, the IR spectrum quality can be improved. By using proper background reference, high quality absorbance spectra can be acquired and quantitative IR analysis would be possible. More interestingly, the over all mass data is a very accurate

quantitative parameter which can be combined with the IR quantitative analysis to reveal detailed kinetic parameters and hidden reaction mechanism. This integration was only a snapshot of big potentials of a integration approach with multi-dimension simultaneous measurements. A lot more information can be extracted than just a collection of those data because the data of different dimensions are correlated.

5 LITERATURE CITED

1. Wang, Guochao, et al. "Absolute positioning by multi-wavelength interferometry referenced to the frequency comb of a femtosecond laser." *Optics express* 23.7 (2015): 9121-9129.
2. Petrov, I., and B. Šoptrajanov. "Infrared spectrum of whewellite." *Spectrochimica Acta Part A: Molecular Spectroscopy* 31.4 (1975): 309-316.

3. Lawson-Wood, Kathryn, and Ian Robertson. "Study of the Decomposition of Calcium Oxalate Monohydrate using a Hyphenated Thermogravimetric Analyser-FT-IR System (TG-IR)."
4. Rahiman, Mujeebu, et al. "Mineral composition of urinary stones-Quantitative analysis by FTIR Spectroscopy."
5. Rak, J., et al. "Thermodynamics of the thermal decomposition of calcium oxalate monohydrate examined theoretically." *Journal of thermal analysis* 43.1 (1995): 239-246.
6. Cumming, Denis J., et al. "Development of a diffuse reflectance infrared fourier transform spectroscopy (DRIFTS) cell for the in situ analysis of co-electrolysis in a solid oxide cell." *Faraday discussions* 182 (2015): 97-111.
7. Isenberg, Mathew, and Steven SC Chuang. "The Nature of Adsorbed CO₂ and Amine Sites on the Immobilized Amine Sorbents Regenerated by Industrial Boiler Steam." *Industrial & Engineering Chemistry Research* 52.35 (2013): 12530-12539.
8. Yu, Jie, and Steven SC Chuang. "The structure of adsorbed species on immobilized amines in CO₂ capture: An in situ IR study." *Energy & Fuels* 30.9 (2016): 7579-7587.
9. Stevens, Robert W., and Steven SC Chuang. "In situ IR study of transient CO₂ reforming of CH₄ over Rh/Al₂O₃." *The Journal of Physical Chemistry B* 108.2 (2004): 696-703.
10. Guzman, Felipe, Steven SC Chuang, and Cheng Yang. "Role of methanol sacrificing reagent in the photocatalytic evolution of hydrogen." *Industrial & Engineering Chemistry Research* 52.1 (2012): 61-65.

11. Isenberg, Mathew, and Steven SC Chuang. "The Nature of Adsorbed CO₂ and Amine Sites on the Immobilized Amine Sorbents Regenerated by Industrial Boiler Steam." *Industrial & Engineering Chemistry Research* 52.35 (2013): 12530-12539.
12. Hedrick, Scott A., et al. "Transient Infrared Characterization of Oxygen Storage Capability of Ce– Pd/Al₂O₃ Catalyst during NO– CO Reaction." *The Journal of Physical Chemistry B* 107.20 (2003): 4834-4843.
13. Konduru, Mahesh V., Steven SC Chuang, and Xihai Kang. "Probing the reactivity of adsorbed NO species by the CO and H₂ pulse during NO decomposition on Cu-ZSM-5." *The Journal of Physical Chemistry B* 105.44 (2001): 10918-10926.
14. Zhang, Xu, Stanley P. Sander, and John F. Stanton. "Detection of the Far-IR v₁₂ Bending Level in Propargyl: A Complete Set of Fundamentals for an Important Radical." *The Journal of Physical Chemistry A* 116.42 (2012): 10338-10343.
15. Cheng, Timothy C., et al. "Mid-and far-ir spectra of H₅⁺ and D₅⁺ compared to the predictions of anharmonic theory." *The journal of physical chemistry letters* 3.21 (2012): 3160-3166.
16. Weber, Ksenia, et al. "Wavelength Scaling in Antenna-Enhanced Infrared Spectroscopy: Toward the Far-IR and THz Region." *ACS Photonics* 4.1 (2016): 45-51.
17. Jalalabadi, Tahereh, et al. "A TGA study of CO₂ gasification reaction of various types of coal and biomass." *Journal of Mechanical Science and Technology* 30.7 (2016): 3275-3281.

18. Babiński, Piotr, et al. "Kinetics of coal and char oxycombustion studied by TG–FTIR." *Journal of thermal analysis and calorimetry* 113.1 (2013): 371-378.

19. Marks Newman, *Computational Physics*, 2013